Deliverable No. 4: Project K5/2338/1

Progress Report 3: Calibration of remote sensing data with surface energy balance data

Quantification of transmission processes along the Letaba River for improved delivery of environmental water requirements (Ecological Reserve)

S Gokool [1], ES Riddell [1,2], C Jarmain [3], A Swemmer [4]

with assistance from R Lerm[4]

1 Centre for Water Resources Research, University of KwaZulu-Natal
2 Conservation Management, South African National Parks
3 Independent Researcher, Stellenbosch
4 SAEON Ndlovu Node, Phalaborwa

February 2016

Table of Contents

List of Figures

List of Tables

1. INTRODUCTION

This deliverable report stems from the non-solicited Water Research Commission (WRC) research project K5/2338 titled:

Quantification of transmission processes along the Letaba River for improved delivery of environmental water requirements (Ecological Reserve)

This report covers progress to date in terms of the river reaches total evaporation results & SW-GW connectivity determination at the Letaba River Transmission Losses study site (Figure 1.1).

This report presents data collected since the submission of previous deliverable 3 (July 2015), and includes:

- A draft manuscript on the approach for downscaling evapotranspiration data derived from satellite information and applied at the scale of the selected river reach in the Letaba river. This is based on the eddy-covariance campaign from May to October 2015 to determine daily ET in Letaba river between Mahale and Letaba Ranch weirs, within two surrounding land use types: emerging farming land and pristine protected area.
- A report on the open water evaporation calculation during the above mentioned campaign.
- A report on soil water evaporation measurements conducted at selected time intervals in accordance with the above.
- Nearby weather station parameters during the above and assessment of spatio-temporal trends.
- Correlation of mass balance approach to estimate evapotranspiration in the river reach with the downscaled ET data.

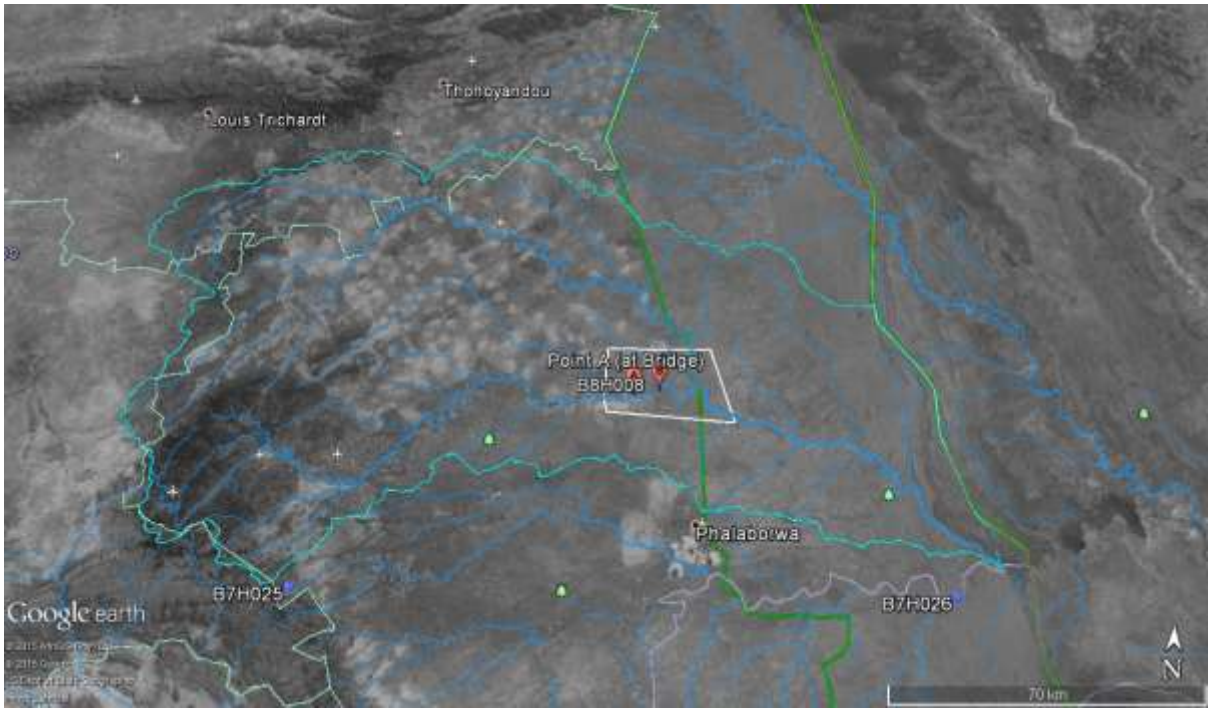

Figure 1.1 The location of the Transmission Losses study site within the Letaba catchment

2. QUANTIFYING RIPARIAN TOTAL EVAPORATION ALONG THE LETABA RIVER: A COMPARISON BETWEEN TWO TECHNIQUES TO ESTIMATE TOTAL EVAPORATION AT A MODERATE SPATIAL RESOLUTION AND A HIGH TEMPORAL RESOLUTION

2.1 Abstract

Riparian vegetation plays a significant role in the interaction between surface water and ground water systems. However, knowledge regarding the water use of riparian vegetation and their associated impacts on groundwater and streamflow transmission losses in South Africa remains fairly limited. Conventional, field-based evaporation estimation approaches can be used to quantify riparian total evaporation. However, the spatial representativeness of these techniques is often limited, as the estimates are generally site specific or line averaged estimates of total evaporation.

The use of satellite earth observation data for the estimation of spatially representative total evaporation has been well documented and therefore represents a suitable alternative for the estimation of riparian total evaporation if the data can be represented at the suitable spatial resolution. One of the major challenges facing total evaporation modelling through the use of satellite earth observation data, is the trade-off between the spatial and temporal resolution associated with imagery. Coarse spatial resolution imagery, which is frequently available may provide information at a spatial scale which is too great for hydrological applications, whereas moderate spatial resolution imagery, which is ideally suited for the estimation of total evaporation at the field scale is not often available.

The objective of this paper was to assess the feasibility of two techniques, to estimate total evaporation at both a moderate spatial resolution and a high temporal resolution. The Surface Energy Balance System (SEBS) Model was used to derive daily total evaporation from Landsat and MODIS images. Two approaches; the $K_{c\ act}$ approach and downscaling with linear regression were evaluated by comparing their respective total evaporation estimates against the original SEBS total evaporation estimates derived using Landsat, as well as total evaporation estimates acquired from an Eddy covariance flux tower. The results of this study showed that while both techniques were able to provide estimates consistent with the original SEBS total evaporation estimates derived using Landsat, there was a fairly poor correlation with the *in-situ* total evaporation estimates.

2.2 Introduction

Riparian vegetation plays a significant role in the interaction between surface water and ground water systems, as it influences the recharge of aquifers, either directly by extracting ground water, or indirectly by altering the flow path of precipitation to the water table in recharge zones (LeMaitre *et al.*, 1999).

While, the significance of riparian vegetation water use has been acknowledged, there remains a paucity of research on the water use of riparian species in South Africa (Le Maitre *et al.*, 1999; Schachtshneider, 2010). It is imperative that the knowledge regarding interactions between surface water and groundwater systems is expanded upon, in order to facilitate the sustainable use of South Africa's limited fresh water resources, especially groundwater resources (Le Maitre *et al.*, 1999). According to Hughes (2008), one such area which necessitates the need for our current knowledge to be expanded upon, is the relationship between streamflow transmission losses (TL) and riparian total evaporation.

Riparian total evaporation is often ignored or inadequately represented in TL estimation procedures, which is largely attributable to infiltration-based losses possessing a relatively larger contribution to TL (Cataldo *et al.*, 2010; Shanafield and Cook, 2014). However, the failure to quantify the losses associated with riparian total evaporation can introduce uncertainty into TL estimates. This is particularly pertinent to environments where total evaporation is a considerably large component of the water cycle (Everson, 2001; McKenzie, 2001; Shanafield and Cook, 2014). Consequently the accurate quantification of riparian total evaporation in these environments can facilitate the improved estimation of TL.

There exist a number of techniques and instrumentation accessible to researchers for the estimation of total evaporation. Conventional approaches, such as micro-meteorological techniques have been extensively applied and have proven to be invaluable in furthering our understanding of the role which total evaporation plays in various environmental processes (Jarmain *et al.*, 2009b). However these techniques are only able to provide site specific or line averaged estimates of total evaporation (Lu *et al.*, 2013; Liou and Kar, 2014; Mengistu *et al.*, 2014; Zhuo *et al.*, 2014). Consequently, the estimates which are obtained are only representative of localised conditions and cannot be easily extended to provide estimates of total evaporation over larger areas, unless similar conditions exist (Bastiaansen *et al.*, 2012; Jassas *et al.*, 2015).

It would prove to be impractical and relatively costly to create a network of *in-situ* measurements which can be used to provide representative large scale total evaporation estimates (Elhaddad and Garcia, 2008; Bastiaansen *et al.*, 2012). The use of satellite earth observation provides a potential solution to the spatial limitations associated with conventional total evaporation estimation techniques. Previous research has shown that satellite earth observation holds a great deal of promise, in the provision of useful information, for the quantification of various hydrological processes such as precipitation, soil moisture and total evaporation (van Dijk and Renzullo, 2011; Fern´andez-Prieto *et al.*, 2012; Xu *et al.*, 2014). Satellite earth observation enables representative information to be captured for large geographic scales, as well as data scarce regions, at near real time if data

is captured within those areas. Furthermore, the periodic updating of information, allows for invaluable time series compilations of data.

The advantages of utilizing satellite earth observation data for the estimation of total evaporation have been well documented. The availability of free imagery from sensors such as Moderate Resolution Imaging Spectrometer (MODIS) and Landsat, coupled with higher computing power have facilitated the quantification of spatially distributed total evaporation (Bhattarai *et al.*, 2015). This information has proved to be invaluable for the monitoring and preservation of environmental, hydrological and agricultural systems (Singh *et al.*, 2014b).

One of the major challenges facing total evaporation modelling through the use of satellite earth observation data, is the trade-off between the spatial and temporal resolution associated with imagery, particularly freely available imagery (Singh *et al.*, 2014b).

Coarse spatial resolution (CSR) imagery can be used for the routine monitoring and estimation of total evaporation due to their high temporal resolution (HTR) (Hong *et al.*, 2011; Ha *et al.*, 2013), however it is often the case that the CSR is too great to provide useful information for hydrological applications, due to pixel sizes exceeding the size of the area under observation (Spiliotopolous *et al.*, 2013; Singh *et al.*, 2014b; Bhattarai *et al.*, 2015). The improved spatial resolution of moderate spatial resolution (MSR) imagery has been recognised, as being ideally suited for the estimation of total evaporation at the field scale to local levels (Anderson *et al.*, 2012; Ha *et al.*, 2013). The continuous advancement in satellite earth observation technologies and capabilities has seen an increase in the demand for MSR total evaporation products for field and catchment scale applications (Bhattarai *et al.*, 2015).

The objective of this paper was to assess the performance of two techniques, a simple downscaling procedure and an infilling approach, to estimate the total evaporation in the riparian zone at both MSR and HTR. For the better assessment of their performance, the total evaporation estimates produced by the aforementioned techniques, were compared against the original SEBS total evaporation estimate derived at the MSR, as well as *in-situ* estimates acquired from an Eddy covariance (EC) flux tower.

2.3 Materials and Methodology

2.3.1 Study area and data sets

The greater study area is situated along a portion of the Groot Letaba River, located in the Letaba catchment in the north-eastern half of South Africa, as depicted in **Error! Reference source not found.**. The predominant vegetation found within and along the riparian zone are *Phragmites Mauritianus*, *Ficus sycomorus* (Fig), *Philonoptera violecia* (Apple leaf) and *Diospyros mespiliformis* (Jackalberry), while agricultural fields, rangelands, as well as alien invasive species are situated adjacent to the riparian zone.

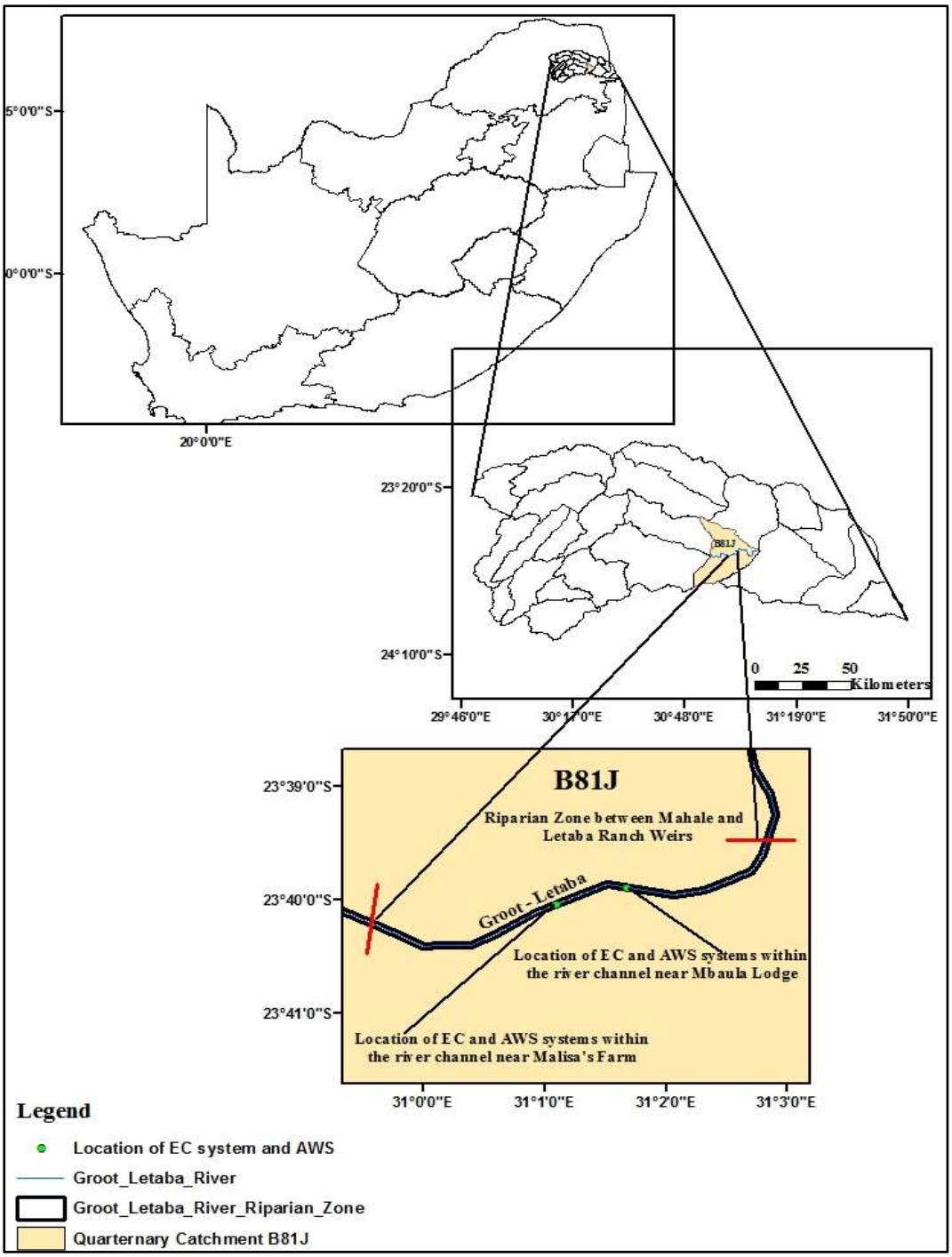

Figure 2-2.1 Location of the study area within the quaternary B81J, situated in the Letaba Catchment

The climate across the catchment can be classified as semi-arid (Strydom *et al.*, 2014) . The catchment receives seasonal rainfall with majority of the rainfall falling in the summer months (Pollard and du Toit, 2011a). According to Katambara and Ndiritu (2010) approximately 40 to 50% of the rainfall generally occurs during January and February. The mean annual precipitation (MAP) is approximately 612 mm (WRC, 2001). Potential evaporation (as measured by A-pan), may exceed the available supply of rainfall, with its effects accentuated in the drier reaches of the catchment (DWAF, 2004). Mean annual temperatures range from 18 ^{0}C in the mountainous regions to 28 ^{0}C in the eastern regions. The elevation of the riparian zone within the study area is approximately 332 m above mean sea level.

A one sensor eddy covariance system was installed at two separate points along the Groot Letaba River between Letaba Ranch and Mahale weirs, during the period of study, falling in the winter season. The system was first setup within the river channel nearby an emerging farming land where grazing is allowed (transect 1) and measurements were acquired from the 17th Jun to 13th Aug 2015. The system was then moved to a pristine protected area where livestock prevented from grazing (transect 2), approximately 1.2 km further upstream within the river and measurements were acquired from the 21st Aug to 22nd Oct 2015.

Error! Reference source not found. provides an illustration of the locations of the EC system within the river channel. The system was situated at these two points in an attempt to capture the total evaporation associated with differing vegetation, bare soil and water compositions within the river channel. The EC total evaporation values were estimated by weighting the contribution of the components of the energy balance according to the coverage of land uses across the area in which the system was situated. The weighting of EC total evaporation estimates was done as follows for transect 1; (i) 20% water contribution, (ii) 40% for bare soil and (iii) 40% for vegetation. The weighting of EC total evaporation estimates was done as follows for transect 2; (i) 20% water contribution, (ii) 20% for bare soil and (iii) 60% for vegetation.

The EC measurements were taken in parallel with the acquisition and processing of the satellite earth observation data, so that the *in-situ* estimates of total evaporation could be used to validate total evaporation estimates derived from satellite earth observation data.

Clear sky Landsat 7 and 8 Level 1 Geotiff products, as well as MODIS Level 1 B Terra images from the 17th June to 22nd October 2015 were selected to estimate total evaporation using the SEBS Model. The pre-processing of images were conducted, using ILWIS and the MODIS Swath Tool, based on the procedures outlined in Su and Wang (2013), Singh *et al*. (2014a) and USGS (2015). The images were used as inputs to the SEBS Model in conjunction with meteorological data, to estimate total evaporation.

2.4 The Simplified Surface Energy Balance System (SEBS)

The SEBS Model was selected for application in this study, as it has been extensively applied for the estimation of regional fluxes and total evaporation and has been shown, to provide accurate estimates of total evaporation and terrestrial heat fluxes (Jarmain *et al.*, 2009a; Yang *et al.*, 2010; Zhuo *et al.*, 2014). The conceptualization of the SEBS Model is discussed in Su (2002). SEBS estimates atmospheric turbulent fluxes using both satellite earth observation and spatially representative meteorological data (Su, 2002; Liou and Kar, 2014; Pardo *et al.*, 2014).

The model estimates land surface physical parameters from spectral reflectance and radiance (Su *et al.*, 1999), a comprehensive model for the approximation of the roughness length of heat transfer (Su *et al.*, 2001) and an innovative procedure for the estimation of the evaporative fraction on the basis of the energy balance at limiting cases (Su, 2002). The model applies the shortened surface energy balance equation to partition the available energy into sensible and latent heat flux density. The daily total evaporation is estimated, assuming the evaporative fraction remains constant throughout the day (Su, 2002).

SEBS was applied in this study, using satellite earth observation data acquired from Landsat (7&8) and MODIS to estimate total evaporation for the riparian zone along the Letaba River. The spatial resolution of the SEBS total evaporation estimate is dependent on the spatial resolution of the thermal band (Su, 2002; Alidoost *et al.*, 2015). Moderate spatial resolution (MSR) imagery acquired by Landsat 7&8 provides thermal bands at a spatial resolution of 60m and 100 m, respectively, which are resampled to 30 m and possess a temporal resolution of 16 days, however; data can be obtained with an 8 day gap between consecutive data acquisitions, if data from both Landsat 7&8 is available and used (USGS, 2015). Coarse spatial resolution imagery acquired by MODIS provides thermal bands at a spatial resolution of 1 km and a temporal resolution of 16 days.

To obtain a complete daily ET record for the riparian zone along the Letaba River, for the measurement period (17th June 2015 to 22nd October 2015) at MSR, a combination of two approaches were followed: (a) a linear regression downscaling approach and (b) the an infilling approach using $K_{c\ act}$ and reference ET to infill missing data.

2.5 Spatial Downscaling of Satellite Derived Total Evaporation

The application of downscaling procedures are used to facilitate the amalgamation of the advantages of HTR imagery with MSR imagery. Bierkens *et al.* (2000) and Liang (2004) define downscaling as the increase in spatial resolution resulting from the disaggregation of the original dataset. Downscaling procedures attempt to restore spatial variations at a particular scale, by assuming the values at the larger scale represent the average of the values at the smaller scale (Bierkens et al., 2000).

The procedure results in an increase of the number of pixels within an image, with the output of each pixel representing a smaller area (Hong *et al*., 2011). According to Ha *et al*. (2013) and Spiliotopolous *et al*. (2013) downscaling procedures can be broadly classified into two categories; (i) scale based traditional downscaling and (ii) pan sharpening or data fusion techniques.

In this study, a relatively simplistic downscaling procedure predicated upon a linear regression discussed in Hong *et al*. (2011) was tested to provide total evaporation estimates at a MSR with HTR, as it has been shown by Hong *et al*. (2011) and Spiliotopolous *et al*. (2013) to provide results within acceptable limits.

The regression approach disaggregates CSR imagery by applying a linear regression between two CSR images to a preceding or subsequent MSR image covering the same area of interest (Hong *et al*., 2011). It is assumed that the linear relationship between CSR imagery remains valid between MSR imagery (Hong *et al*., 2011).

In order, to create a daily continuous MSR total evaporation dataset for the period of investigation in this study, a linear regression was initially applied between two consecutive MODIS total evaporation estimates (M_1 and M_2) generated, using the SEBS Model, to obtain regression coefficients. These coefficients were then applied to the Landsat total evaporation image (L_1) generated using the SEBS Model for the same date as the first MODIS total evaporation image (M_1), in order to generate a total evaporation image (L_2) at the Landsat spatial resolution, for the same date as the subsequent MODIS total evaporation image (M_2).

This procedure was repeated, however; the linear regression was then performed between the MODIS total evaporation image for day one (M_1) and the MODIS total evaporation image for day three (M_3) to obtain regression coefficients. These coefficients were then applied to the Landsat total evaporation image (L_1) obtained for the same date as the first MODIS total evaporation image (M_1), in order to generate a total evaporation image (L_3) at the Landsat spatial resolution, for the same date as the subsequent MODIS total evaporation image (M_3).

This procedure was systematically repeated, until a new Landsat Level 1 Geotiff product was available. Once this product was available, the abovementioned procedure was repeated. Figure 2.2 and Figure 2.3 provide a schematic representation of the abovementioned process to better understand how the daily continuous MSR total evaporation dataset was generated and an example of a downscaled total evaporation map generated for this study, respectively.

Bhattarai *et al*. (2015) notes that the procedures discussed in Hong *et al*. (2011) have not yet been applied to obtain a seasonal continuous MSR total evaporation dataset. Therefore, the results of the investigations conducted in this study can provide valuable insight on the suitability of applying the linear regression approach to generate continuous MSR total evaporation dataset on a daily time step.

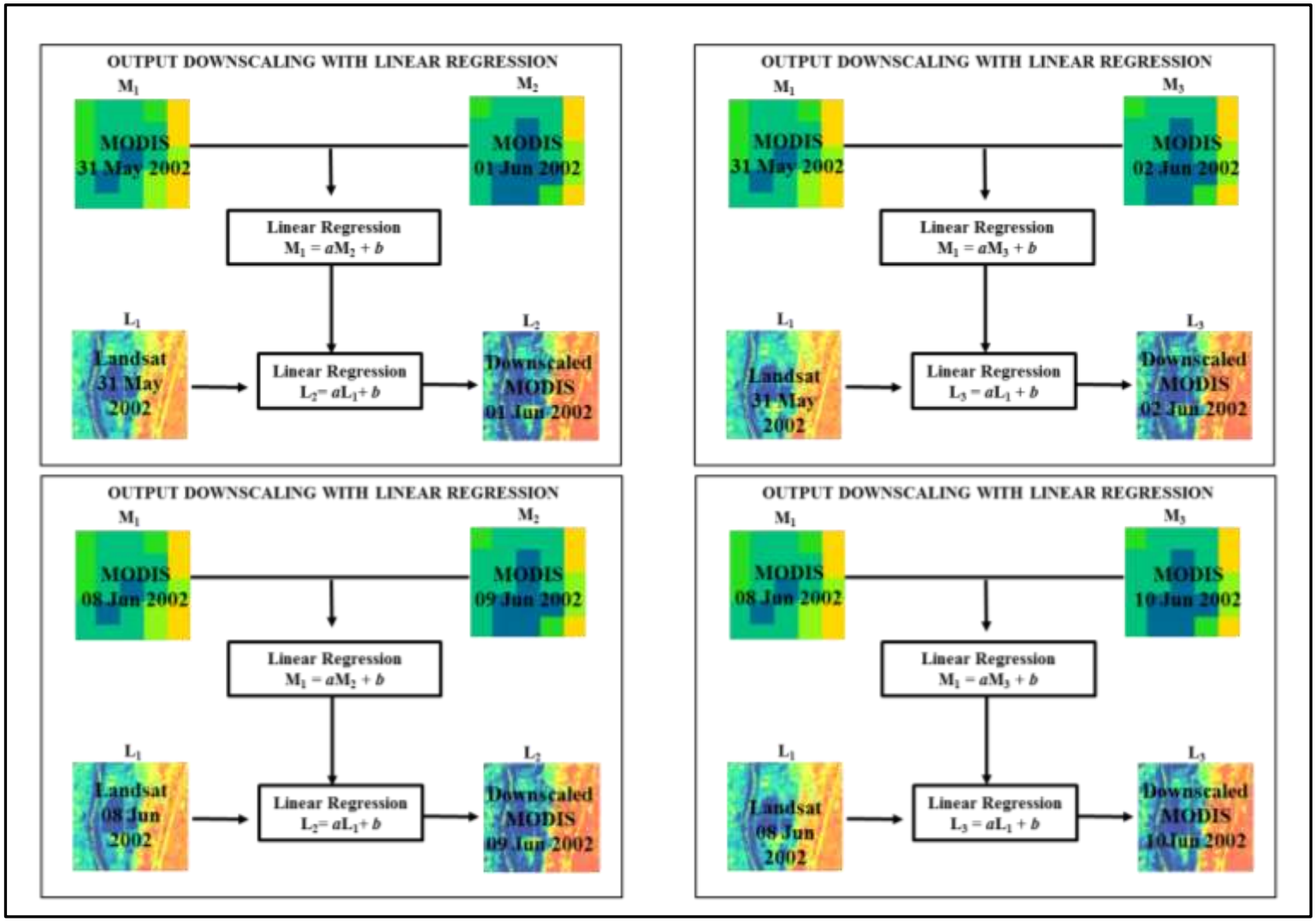

Figure 2.2. Schematic of the downscaling with linear regression approach methodology to create a daily continuous MSR total evaporation dataset, where *a* and *b* are the linear regression coefficients and L_2 and L_3 are the subsequent spatially downscaled total evaporation maps at the Landsat resolution (adapted from Hong *et al.*, 2011)

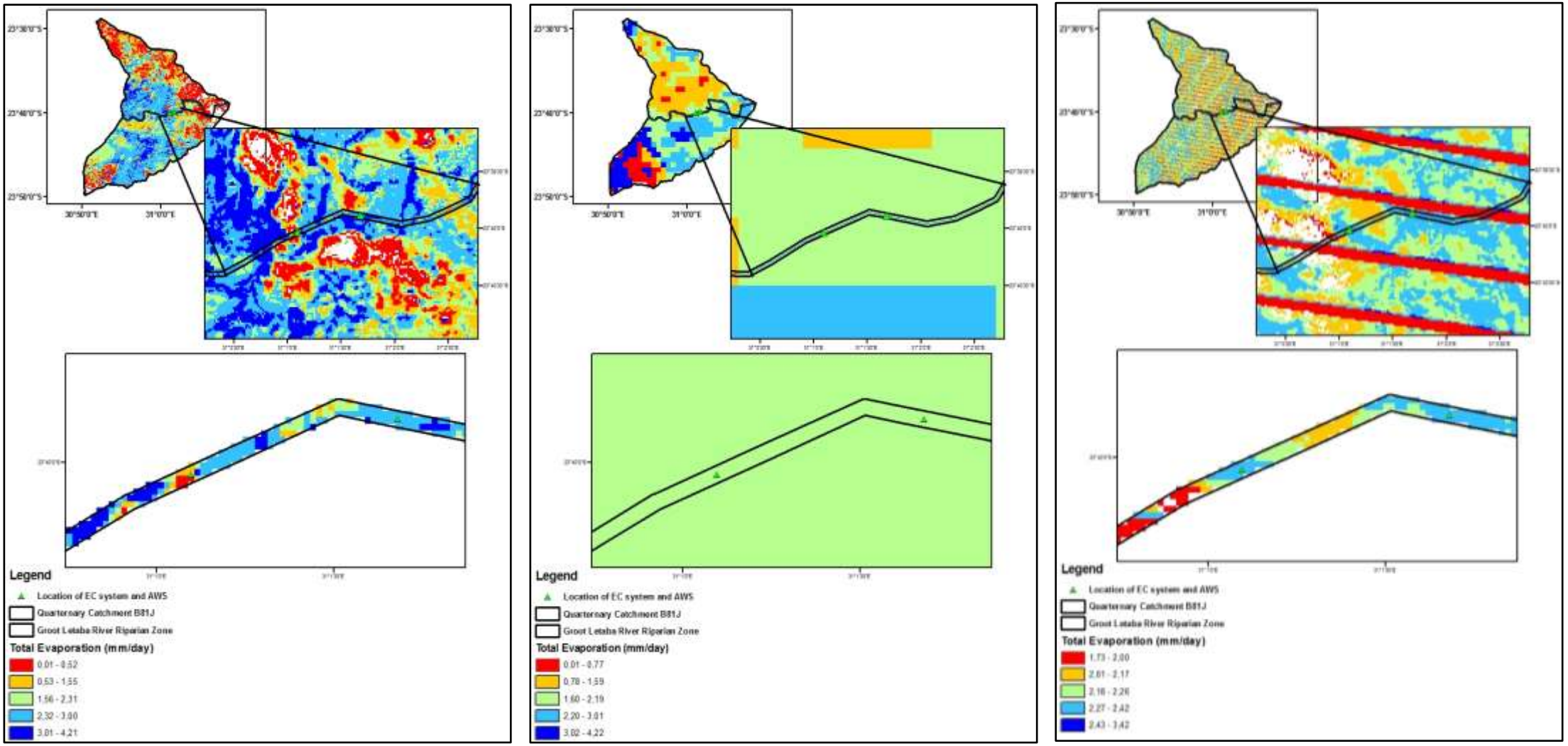

Figure 2.3 An illustration of SEBS total evaporation derived using MODIS and Landsat data for the 07th July 2015 a) SEBS total evaporation map derived using Landsat, b) SEBS total evaporation map derived using MODIS and c) Downscaled total evaporation derived using linear regression

2.6 The $K_{c\ act}$ infilling approach

The $K_{c\ act}$ approach discussed in Santos *et al.* (2008), was applied to generate a daily continuous Landsat total evaporation time series. The actual total evaporation and reference evaporation required for the application of this technique were acquired, respectively, from SEBS total evaporation estimates and FAO Penman-Monteith reference evaporation derived from meteorological data collected for the study area. The calculation of $K_{c\ act}$ is given as:

$$K_{c\ act} = \frac{ET_a}{ET_{ref}} \quad (1)$$

Where $K_{c\ act}$ can be defined as the actual crop coefficient which accounts for the effects of environmental stress (Allen *et al.*, 2005b), ET_a is the total evaporation (mm d^{-1}) and ET_{ref} is the grass reference evaporation determined using the FAO Penman-Monteith reference evaporation approach (mm d^{-1}). The advantage of utilising the $K_{c\ act}$ approach is that; (i) it is a physically based approach, (ii) it is relatively simplistic to apply with fairly short processing times and (iii) total evaporation estimates extending from only one satellite earth observation data set is required.

The application of the $K_{c\ act}$ approach is predicated on the assumption that the conditions which are use used to derive $K_{c\ act}$ remain the same for the period in which it is applied. Furthermore, spatially representative meteorological data is required for the determination of the FAO Penman-Monteith reference evaporation, in order to estimate spatially representative total evaporation.

Thirteen useable Landsat (7&8) Level1 Geotiff products were available during the study period. $K_{c\ act}$ values were determined as the ratio between the SEBS total evaporation derived using Landsat and ET_{ref}. These values were then used to develop a $K_{c\ act}$ curve. An exponential curve was generated, to interpolate values between images so that the temporal progression of $K_{c\ act}$ can be accounted for (Santos *et al.*, 2008). The $K_{c\ act}$ curve generated for the study period is represented in Figure 2.4. The $K_{c\ act}$ values were used in conjunction with ET_{ref} to estimate ET_a for the study period.

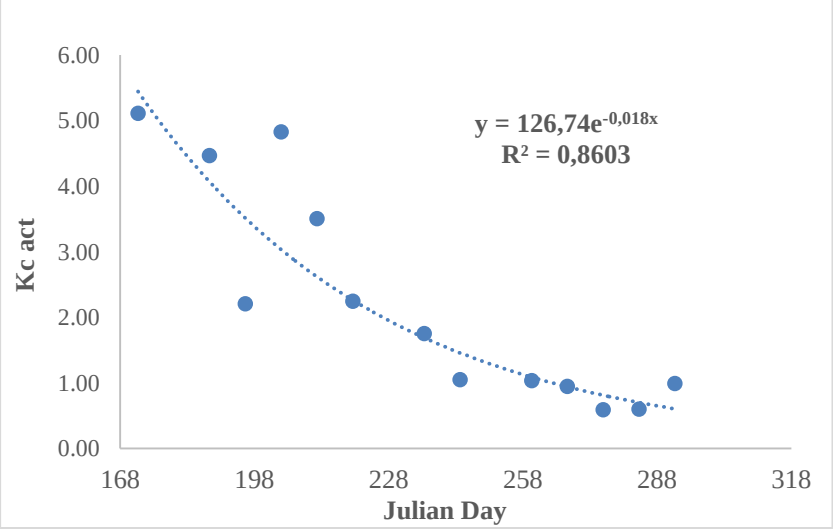

Figure 2.4 $K_{c\ act}$ curve derived using SEBS total evaporation estimate and ET_{ref} for the period 17th Jun to 22nd Oct 2015

2.7 Results and Discussion

The downscaled total evaporation estimates and the total evaporation estimated using $K_{c\ act}$ were compared to the original SEBS total evaporation estimates derived using Landsat (7 and 8), as well as the *in-situ* total evaporation estimates. The satellite pixels located, in and around, the EC flux tower were selected as areas of interest and only the data within these pixels were used for data comparisons.

2.7.1 Landsat Total Evaporation vs Infilled Total Evaporation vs Downscaled Total Evaporation

The estimates obtained using the $K_{c\ act}$ approach compared favourably to the original SEBS total evaporation estimate derived using Landsat. Table 3.1 indicates the results of the investigations.

The relative volume error between the $K_{c\ act}$ total evaporation estimates and the original SEBS total evaporation estimates derived using Landsat, indicates that on average the $K_{c\ act}$ approach over-estimated total evaporation by approximately 11%. The Mean Absolute Difference and RMSE values are 0.6 mm day^{-1} and 0.86 mm day^{-1}, respectively. These statistics, as well as the results of the t-test indicate a fairly good agreement between the $K_{c\ act}$ total evaporation estimates and the original SEBS total evaporation estimates derived using Landsat and show no significant difference between their means.

The estimates obtained using the downscaling with linear regression approach compare favourably to the SEBS total evaporation estimate derived using Landsat. Table 2.1 indicates the results of the investigations. The relative volume error between the downscaled total evaporation estimates and the SEBS total evaporation estimates derived using Landsat, indicates that on average the downscaling with linear regression approach under-estimated total evaporation by approximately 5%. The Mean Absolute Difference and RMSE values are 1.21 mm day^{-1} and 1.41 mm day^{-1}, respectively.

These statistics, as well as the results of the t-test indicate a fairly good agreement between the downscaled total evaporation estimates and the SEBS total evaporation estimates derived using Landsat and show no significant difference between their means.

It should be noted that while the downscaled total evaporation estimate (L_2) may compare favourably with the original SEBS total evaporation estimates derived using Landsat, upon visual examination there are noticeable differences in the spatial distribution of total evaporation, as seen in Figure 2.4. The downscaled total evaporation map (L_2) will adopt the spatial distribution characteristics of the subsequent SEBS total evaporation map (L_1) derived using Landsat, as it is used as an input for the downscaling procedure. Hence, the striping

seen in the downscaled total evaporation map (L_2) presented in Figure 2.4, as a Landsat 7 image was used for derivation of the SEBS total evaporation map (L_1). The striping seen in the Landsat 7 ETM+ imagery post May 31st 2003, is associated with the failure of the Scan Line Corrector (SLC). Since then Landsat 7 ETM+ imagery is collected in "SLC-off" mode. Approximately, 22% of any given scene is lost due to this error (USGS, 2015).

Table 2.1 A comparison of SEBS total evaporation using Landsat, $K_{c\ act}$ derived total evaporation and downscaled total evaporation for the 13 days in which useable Landsat Level 1 Geotiff imagery was available

	Original Landsat (7 and 8) ET (mm)	**Landsat Infilled, using $K_{c\ act}$ (mm)**	**MODIS Downscaled ET (mm)**
Total	39.30	42.28	35.23
Average	3.02	3.25	2.71
Max	4.10	5.08	5.59
Min	1.60	1.97	1.60
Median	3.32	3.44	2.37
Variance	0.61	0.97	2.06
Std Dev	0.80	0.99	1.39
RVE		-10.81	5.36
MAD		0.68	1.21
RMSE		0.86	1.41
T-test (p value)		0.52	0.84

The original SEBS total evaporation estimates derived using Landsat, the $K_{c\ act}$ total evaporation estimates and the downscaled total evaporation estimates were accumulated for the 13 days in which useable Landsat Level 1 Geotiff imagery was available and are illustrated in Figure 2.5. Both the $K_{c\ act}$ total evaporation estimates and the downscaled total evaporation estimates appear to be in fairly good agreement with the original SEBS total evaporation estimates derived using Landsat for the 13 days in which useable Landsat Level 1 Geotiff imagery was available. The two approaches are able to capture the trends of the original SEBS total evaporation estimates derived using Landsat.

The results of the investigations presented in Table 2.1 and illustrated in Figure 2.5, indicate that both the $K_{c\ act}$ and the downscaling with linear regression approach can be used to derive daily total evaporation estimates at a MSR, with reasonable accuracy.

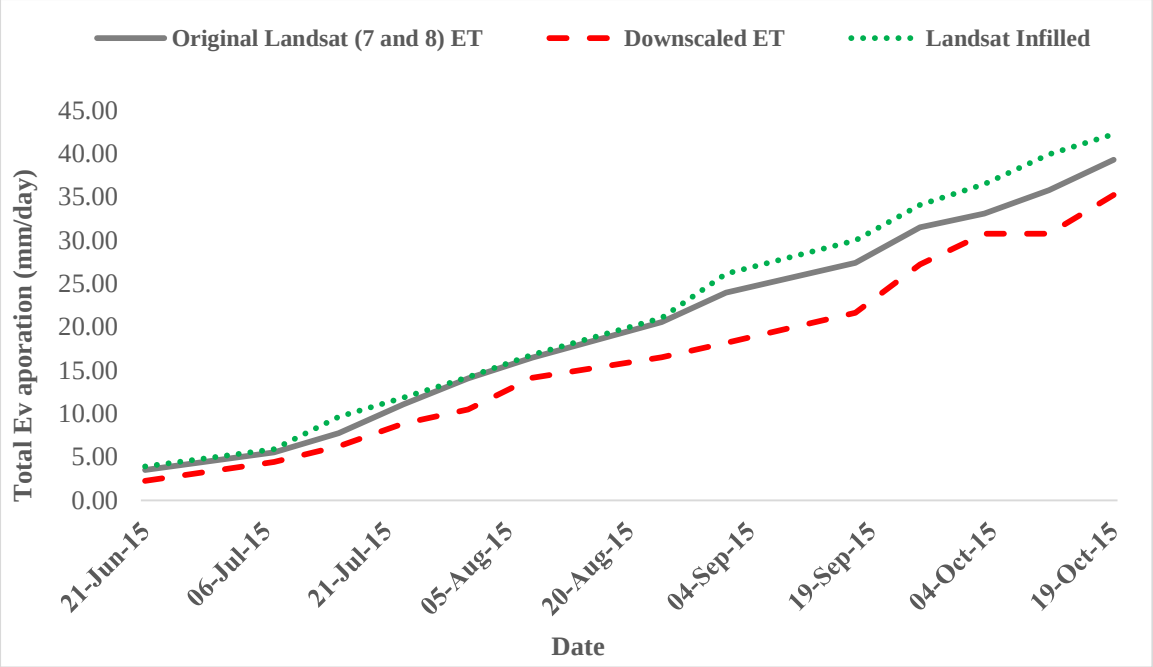

Figure 2.5 A comparison of accumulated SEBS total evaporation estimates derived using Landsat, the $K_{c\ act}$ total evaporation estimates and the downscaled total evaporation estimates

2.8 A comparison of satellite derived total evaporation against total evaporation measured *in-situ* for the period 17th June to 22nd October 2015

The $K_{c\ act}$ and the downscaling with linear regression approach were used to derive daily total evaporation estimates during the period 17th June to 22nd October 2015. These estimates were then compared to the *in-situ* estimates of total evaporation acquired from the EC flux tower. A summary of the comparisons between the satellite derived total evaporation estimates and total evaporation measured at transect 1 for the period 17th Jun to 13th Aug 2015 and at transect 2 for the period 21st August to 22nd October 2015 is provided in

Table **2.2** and Table 2.3. In general, the satellite derived total evaporation estimates were found to be higher than the *in-situ* total evaporation estimates, as illustrated in Figure 2.6.

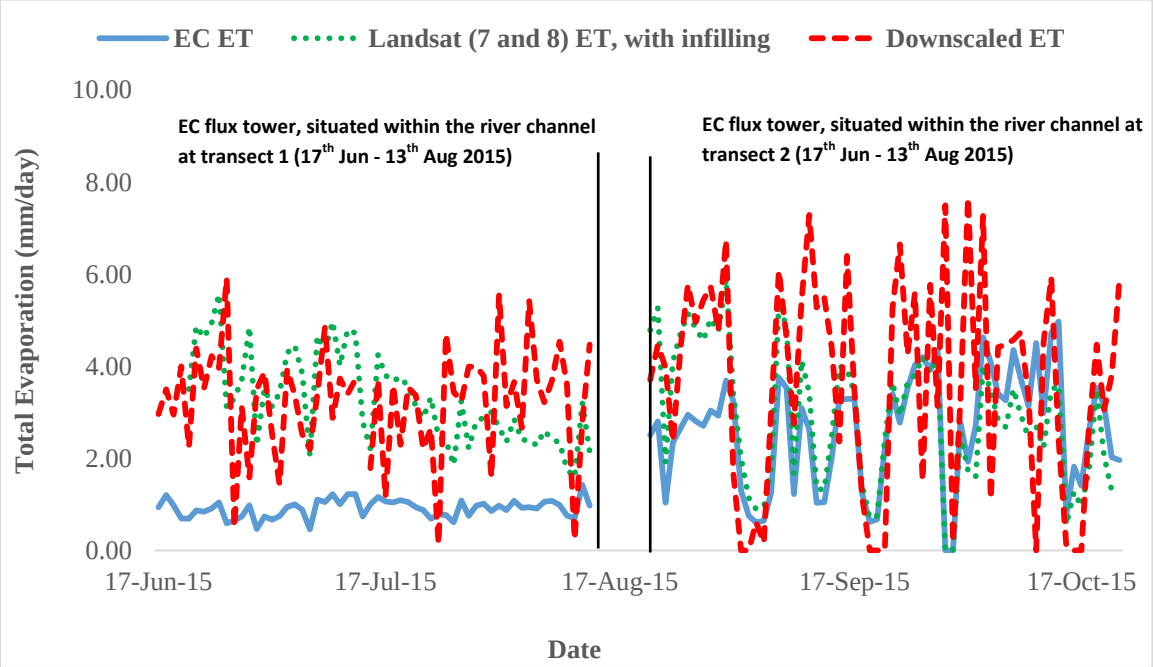

Figure 2.6 A comparison of *in-situ* total evaporation estimates acquired from an EC flux tower, the $K_{c\ act}$ total evaporation estimates and the downscaled total evaporation estimates for the period 17th June to 22nd October 2015

As stated previously, the EC flux tower was installed at two separate points along the Groot Letaba River between Letaba Ranch and Mahale weirs, during the period of study. The rationale for situating the EC flux tower at the two different locations within the river channel during the period of study was to assess how differing vegetation, bare soil and water compositions within the river channel would influence the total evaporation measured *in-situ*.

The contribution of vegetation, sand and water within the river channel is markedly different between the two areas (transect 1 and transect 2). Although, the type of vegetation within the river channel at these two locations is fairly similar, the density of actively growing vegetation within the river channel for the protected area is greater. This is chiefly, due to livestock being prevented from entering the protected area by an electric barrier, therefore they are unable to graze on the vegetation present within the channel.

The temporal progression of meteorological factors which influence total evaporation rates, as well as differences in the contribution of vegetation, sand and water within the river channel between the two areas, contributed significantly to the total evaporation measured *in-situ*. The results presented in Figure 2.6, as well as

Table **2.2** and Table 2.3 indicate that the discrepancies between the satellite derived total evaporation estimates and the *in-situ* total evaporation estimates were higher for transect 1.

Table 2.2 A comparison of SEBS total evaporation using Landsat, $K_{c\ act}$ derived total evaporation and downscaled total evaporation for the period 17th June to 13th August 2015

	EC ET (mm)	Landsat (7 and 8) ET, with infilling (mm)	MODIS Downscaled ET (mm)
Total	52.92	178.13	183.96
Average	0.91	3.30	3.23
Max	1.42	5.57	5.91
Min	0.46	1.59	0.14
Median	0.94	3.17	3.44
Variance	0.04	0.98	1.43
Std Dev	0.20	0.99	1.20
RVE		-244.74	-260.40
MAD		2.29	2.33
RMSE		2.48	2.57
T-test (p value)		1.87E-24	5.63E-21

Table 2.3 A comparison of SEBS total evaporation using Landsat. $K_{c\ act}$ derived total evaporation and downscaled total evaporation for the period 21st August to 22nd October 2015

	EC ET (mm)	Landsat (7 and 8) ET. with infilling (mm)	Downscaled ET (mm)
Total	164.80	181.00	229.57
Average	2.62	2.87	3.64
Max	3.16	2.05	5.89
Min	1.96	1.23	3.06
Median	2.02	1.29	3.80
Variance	0.45	0.21	2.15
Std Dev	0.67	0.46	1.47
RVE		36.22	-98.88
MAD		0.78	1.87
RMSE		1.04	0.01
T-test (p value)		0.20	5.63E-21

Lower total evaporation estimates are captured by the EC flux tower within transect 1. as illustrated in Figure 2.6 and

Table **2.2**. The atmospheric demand for water vapour is generally lower during this period as illustrated in Figure 2.7. Furthermore. the EC total evaporation values were estimated by weighting the contribution of the components of the energy balance according to the coverage of land uses across the area in which the system was situated. There is a lower density of actively growing vegetation within the river channel at this location. as livestock are allowed to freely roam the river channel and often graze on the vegetation present here.

The weighting of the EC total evaporation estimates at this location. accounts for an equal contribution of vegetation and bare soil. Consequently. the lower atmospheric demand for water vapour and the influence associated with a greater contribution of bare soil. resulted in lower total evaporation estimates acquired at this location.

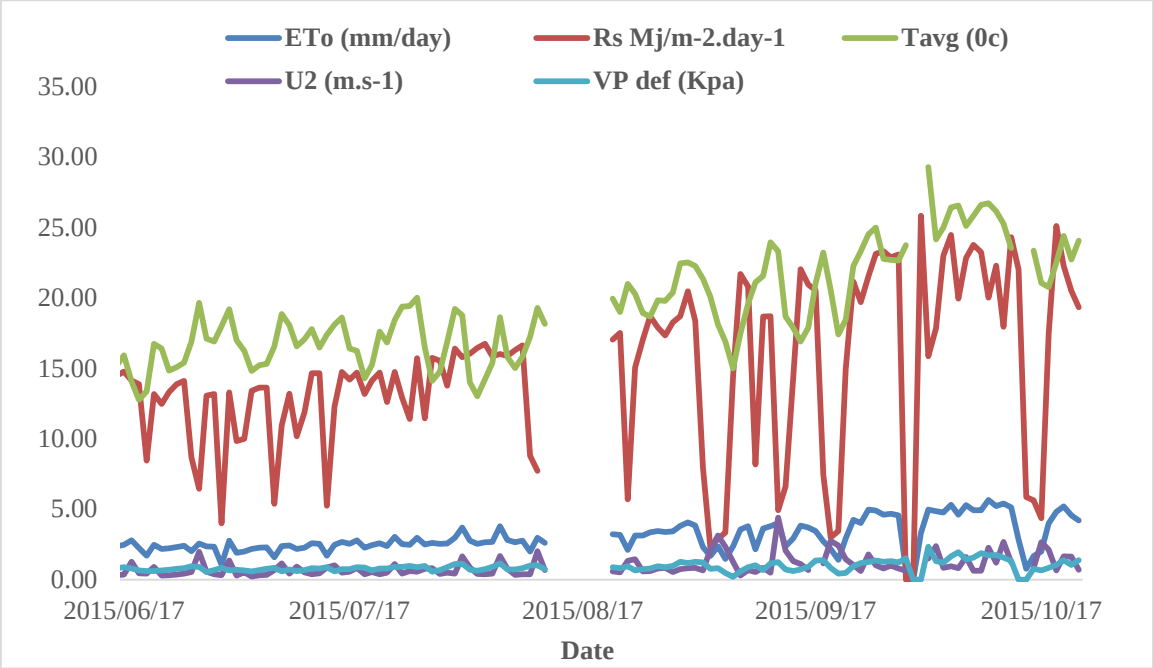

Figure 2.7 A representation of the meteorological factors influencing the atmospheric demand for water vapour within transects 1 and 2. for the period period 17th June to 22nd October 2015

Higher total evaporation estimates are captured by the EC flux tower within transect 2. as illustrated in Figure 2.6 and 3. The atmospheric demand for water vapour is generally higher during this period as illustrated in Figure 2.7. Furthermore. the density of actively growing vegetation within transect 2 is higher. due to livestock being prevented from entering this area. The weighting of the EC total evaporation estimates at this location. accounts for a larger contribution of vegetation and a lower contribution from bare soil. Accordingly. the total evaporation estimates being captured by the EC flux tower at this location are higher.

Subsequently. the general degree of over-estimation associated with the comparisons between the satellite derived total evaporation estimates and the EC total evaporation

estimates. was further exacerbated for the period in which. the *in-situ* measurements were taken at transect 1.

Furthermore. the higher degree of uncertainty generally associated with the SEBS total evaporation estimates during cooler and dryer periods (Gokool. 2014; Timmermans. 2014). could also have influenced the discrepancies found between the *in-situ* total evaporation and satellite derived total evaporation estimates at the two locations of the EC flux tower. The results presented have shown that the discrepancies between the $K_{c\ act}$ total evaporation estimates. the downscaled total evaporation estimates and *in-situ* total evaporation estimates were highest during the cooler dryer periods of the study.

Both the $K_{c\ act}$ and the downscaled total evaporation estimates are generated from the original SEBS total evaporation estimates derived using Landsat and MODIS imagery. it can therefore be expected that uncertainties associated with these estimates. will be introduced to the total evaporation estimates generated by the $K_{c\ act}$ and the downscaling with linear regression approaches.

The general degree of over-estimation between comparisons of the *in-situ* total evaporation estimates. the $K_{c\ act}$ total evaporation estimates and the downscaled total evaporation estimates for the entire study period. can be attributed to the complexity of applying the aforementioned techniques correctly under heterogeneous conditions within the study area. The footprint of the EC flux tower is limited due its location. Much of the area in which the flux tower is situated. is lower than the surrounding areas. Consequently. the total evaporation estimates which are captured represent a particular contribution of vegetation. sand and water within the river channel and may not capture the contribution of riparian vegetation situated higher up along the river banks.

The total evaporation estimates obtained by applying the $K_{c\ act}$ and the downscaling with linear regression approach. are largely influenced by the spatial resolution of the Landsat and MODIS imagery used to derive the original SEBS total evaporation estimates. respectively.The satellite derived total evaporation estimates are able to capture the contribution of riparian vegetation within the river channel. as well as along the river banks.

Hence. the probability of the satellite derived total evaporation estimates generally being larger than the *in-situ* measurements can be expected for the study area. This can be further supported by the data displayed in Figure 2.8. which shows the *in-situ* total evaporation estimates and the original SEBS total evaporation estimates derived using Landsat and MODIS.

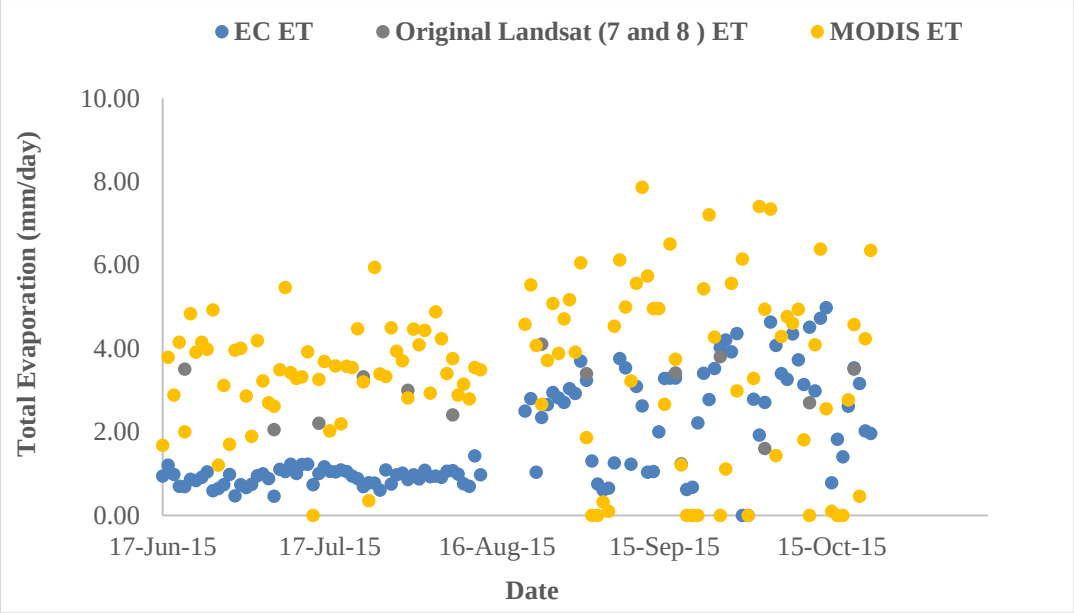

Figure 2.8 A comparison of accumulated *in-situ* total evaporation estimates acquired from an EC flux tower and satellite derived total evaporation using Landsat and MODIS data for the period 17th June to 22nd October

While both the $K_{c\ act}$ and the downscaled total evaporation estimates have largely over-estimated total evaporation when compared to the *in-situ* total evaporation estimates. the degree of over-estimation is higher for the downscaling approach.

This occurrence can be attributed to the nature of the SEBS total evaporation estimates derived using MODIS during this period. The SEBS total evaporation derived using MODIS was generally higher than the *in-situ* total evaporation, as well as the SEBS total evaporation derived using Landsat. As. the spatial resolution of MODIS is 1 km. there is potentially a greater contribution of other land covers being encompassed within the total evaporation estimate. The downscaled total evaporation estimate is dependent on the regression and slope of the two SEBS total evaporation images derived using MODIS (Hong *et al*.. 2011). Consequently. the downscaled total evaporation estimate is largely influenced by the total evaporation captured at the MODIS spatial resolution.

Furthermore. Hong *et al*. (2011) noted that the downscaling with regression approach does not perform well for abrupt changes (greater than 20%) in total evaporation and other surface parameters. Therefore. the downscaled estimates derived using the aforementioned approach may prove to be inadequate for regions experiencing dynamic temporal changes over a short period of time (Hong *et al*.. 2011).

The use of the $K_{c\ act}$ approach is strongly dependent on the relationship between the original SEBS total evaporation estimate derived using Landsat and the FAO Penman-Monteith Reference evaporation. The degree of over-estimation between the original SEBS total evaporation derived using Landsat and the *in-situ* total evaporation estimates for the same day is lower than the degree of over-estimation between the original SEBS total evaporation derived using MODIS and the *in-situ* total evaporation estimates for the same day. Due to the nature of this relationship and the use of FAO Penman-Monteith Reference evaporation. the infilled values using the $K_{c\ act}$ approach were lower.

2.9 Conclusion

In this paper, two procedures the $K_{c\ act}$ infilling approach and a simple downscaling with linear regression approach were presented and compared. These methods were used to predict the daily total evaporation at a MSR for the riparian zone situated along a portion of the Groot Letaba River. The $K_{c\ act}$ and the downscaled total evaporation estimates were evaluated by comparison with the original SEBS total evaporation estimates derived using Landsat (7 and 8). as well as the *in-situ* total evaporation estimates acquired from the ET flux tower.

Both the $K_{c\ act}$ infilling and downscaling with linear regression approaches were found to perform well. as the aforementioned approaches were able to produce estimates. which were consistent with the original SEBS total evaporation estimate derived using Landsat. The results presented in this investigation indicated that. these methods could be applied to predict the daily total evaporation at a MSR for the riparian zone.

The comparison between the total evaporation estimates acquired from the application of the $K_{c\ act}$ and linear regression downscaling approaches. against *in-situ* total evaporation estimates acquired from the EC flux tower were less impressive. Both techniques were shown to perform poorly when compared to *in-situ* total evaporation estimates acquired from the EC flux tower. The reason attributed to this poor correlation was essentially due to the temporal progression of meteorological factors which influence total evaporation rates, as well as markedly different contributions of vegetation, sand and water to the EC total evaporation estimate. for the two locations in which the EC flux tower was situated.

Furthermore, the limited spatial representation of total evaporation estimates acquired from the EC flux tower, as well as the higher degree of uncertainty generally associated with the SEBS total evaporation estimates during cooler and dryer periods, could have further exacerbated the discrepancies found between the *in-situ* total evaporation and satellite derived total evaporation estimates.

The potential of applying the $K_{c\ act}$ infilling and downscaling with linear regression approach to estimate daily total evaporation at a MSR has been highlighted by the results of the comparison between the total evaporation estimates obtained through the application of these techniques and the original SEBS total evaporation estimates derived using Landsat.

While, the comparison of estimates proved to be less favourable when compared the *in-situ* total evaporation estimates, the successful application of these techniques should not be discredited. Future investigations should attempt to utilize spatially representative validation data, in order to draw more meaningful comparisons between the techniques used to predict daily total evaporation at a MSR and *in-situ* measurements. Furthering our knowledge in this regard, provides an opportunity to broaden our existing knowledge base and exploit the potential of using satellite earth observation data to better understand and quantify riparian vegetation water use.

REFERENCES

Alidoost, F, Sharifi, MA and Stein. A. 2015. Region and pixel-based image fusion for disaggregation of actual evapotranspiration. *International Journal of Image and Data Fusion*. DOI: 10.1080/19479832.2015.1055834.

Anderson, MC, Allen, RG, Morse, A and Kustas, WP. 2012. Use of Landsat Thermal Imagery in Monitoring Evapotranspiration and Managing Water Resources. *Remote Sensing of Environment* 122: 50–65.

Bastiaansen, WGM, Cheema, MJM, Immerzeel, WW, Miltenberg, IJ and Pelgrum, H. 2012. Surface energy balance and actual evapotranspiration of the transboundary Indus Basin estimated from satellite measurements and the ET Look model. *Water Resources Research*. 48. Issue 11. Article first published online 21 November 2012. W11512. DOI:10.1029/2011WR010482.

Bhattarai, N, Quackenbush, LJ, Dougherty, M and Marzen, LJ 2015. A simple Landsat–MODIS fusion approach for monitoring seasonal evapotranspiration at 30 m spatial resolution. *International Journal of Remote Sensing* 36(1): 115-143.

Bierkens, MFP, Finke, PA and Willigen, DE. 2000. *Upscaling and Downscaling Methods for Environmental Research*. Dordrecht: Wageningen University and Research Centre. Kluwer Academic.

Cataldo, J, Behr, C, Montalto, F and Pierce, RJ. 2010. Prediction of Transmission Losses in Ephemeral Streams. Western U.S.A. *The Open Hydrology Journal* 4: 19-34.

Department of Water Affairs and Forestry. 2004. Internal Strategic Perspective: Luvuvhu/Letaba WMA. *DWAF Report No*: P WMA 02/000/00/0304.

Elhaddad, A, and Garcia, L,A. 2008. Surface energy balance-based model for estimating evapotranspiration taking into account spatial variability in weather. *J. Irrig. Drain. Eng ASCE* 134(6): 681–689.

Everson CS. 2001. The water balance of a first order catchment in the montane grasslands of South Africa. *Journal of Hydrology* 241: 110-123.

Fernández-Prieto, D, van Oevelen, P, Su, Z and Wagner, W. 2012. Advances in Earth observation for water cycle science. *Hydrology and Earth System Science* 16: 543–549.

Gokool, S. 2014. An assessment of satellite derived total evaporation data as a data source to the ACRU hydrological model. Unpublished Msc Thesis. University of KwaZulu Natal. Pietermaritzburg. South Africa.

Ha, W, Gowda, PH and Howell, TA. 2013. A review of downscaling methods for remote sensing-based irrigation management: Part I. *Irrigation Science* 31: 831–850.

Hacker, F. 2005. Model for Water Availability in Semi-Arid Environments (WASA): Estimation of transmission losses by infiltration at rivers in the semi-arid Federal State of Ceara (Brazil). MSc Thesis. University of Potsdam. Germany.

Hong, S. Hendrickx. JMH and Borchers. B. 2011. Down-scaling of SEBAL derived evapotranspiration maps from MODIS (250 m) to Landsat (30 m) scales. *International Journal of Remote Sensing* 32(21): 6457–6477.

Hughes, DA. 2008. Modelling semi-arid and arid hydrology and water resources the Southern African experience. gwadi.org/sites/gwadi.org/files/hughes_L5.pdfand#8206; Hughes. DA. Mallory. SJL and Louw D. 2008. Methods and software for the real-time implementation of the ecological reserve-explanations and user manual. *WRC Report 1582/1/08*.

Jarmain, C, Bastiaansen, W, Mengistu, MG and Kongo, V, 2009b. A Methodology for Near-Real Time Spatial Estimation of Evaporation. *WRC Report No. 1751/1/09*. ISBN 978-1-77005-725-8.

Jarmain, C, Everson, CS, Savage, MJ, Mengistu, MG, Clulow, AD, Walker, S and Gush, MB, 2009a. Refining tools for evaporation monitoring in support of water resources management. *WRC Report No* 1567/1/08. ISBN 978-1-77005-798-2.

Jassas, H, Kanoua, W and Merkel, B. 2015. Actual evapotranspiration in the Al-Khazir Gomal Basin (Northern Iraq) using the Surface Energy Balance Algorithm for Land (SEBAL) and water balance. *Geosciences* 5: 141-159.

Katambara, Z and Ndiritu, JG. 2010. A hybrid conceptual-fuzzy inference streamflow modelling for the Letaba River system in South Africa. *Physics and Chemistry of the Earth* 35(13-14): 582-595.

LeMaitre, DC, Scott, DF and Colvin C. 1999. A review of information on interactions between vegetation and groundwater. *Water SA* 25(2).

Liang, S. 2004. *Quantitative Remote Sensing of Land Surfaces*. New York: JohnWiley and Sons.

Liou, Y and Kar, SK. 2014. Evapotranspiration Estimation with Remote Sensing and Various Surface Energy Balance Algorithm: A Review. *Energies* 7: 2821-2849.

Lu, J, Li, Z, Tang, R, Tang, B, Wu, H, Yang, F, Labed, J and Zhou, G. 2013. Evaluating the SEBS-estimated evaporative fraction from MODIS data for a complex underlying surface. *Hydrological Processes* 27(22): 3139-3149.

McKenzie, RS and Craig. AR. 2001. Evaluation of river losses from the Orange River using hydraulic modelling. *Journal of Hydrology* 241: 62–69.

Mengistu, MG, Everson, CS, Moyo, NC and Savage, MJ. 2014. The validation of the variables (evaporation and soil moisture) in hydrometeorological models. *WRC Report No. 2066/1/13*. ISBN 978-1-4312-0514-1.

Pardo, N, Sanchez, LM, Timmermans, J, Su, Z, Perez, IA and Garcia, MA. 2014. SEBS validation in a Spanish rotating crop. *Agricultural and Forest Meteorology* 195-196: 132-142.

Pollard, S and du Toit, D, 2011b. Towards the sustainability of freshwater systems in South Africa: An exploration of factors that enable and constrain meeting the ecological Reserve within the context of Integrated Water Resources Management in the catchments of the lowveld. *WRC Report No* K8/1711.

Schactschneider, K. 2010. Water sourcing by riparian trees along ephemeral riverbeds. PhD Thesis. University of Cape Town. South Africa.

Shanafield, M and Cook, PG. 2014. Transmission losses. infiltration and groundwater recharge through ephemeral and intermittent streambeds: A review of applied methods. *Journal of Hydrology* 511: 518–529.

Singh, RK, Senay, GB, Velpuri, NM, Bohms, S and Verdin, JP, 2014b. On the Downscaling of Actual Evapotranspiration Maps Based on Combination of MODIS and Landsat-Based Actual Evapotranspiration Estimates. *Remote Sensing* 6: 10483-10509.

Singh, RK, Senay, GB, Velpuri, NM, Bohms, S, Scott, RL and Verdin, JP. 2014a. Actual Evapotranspiration (Water Use) Assessment of the Colorado River Basin at the Landsat Resolution Using the Operational Simplified Surface Energy Balance Model. *Remote Sensing* 6: 233-256.

Spiliotopolous, M, Adaktylou, N, Loukas, A, Michalopoulou, H, Mylopoulos, N and Toulios, L. 2013. A spatial downscaling procedure of MODIS derived actual evapotranspiration using Landsat images at central Greece. Proceedings of SPIE - The International Society for Optical Engineering - August 2013. DOI: 10.1117/12.2027536.

Strydom, T, Riddell, E, Swemmer, A, Nel, JM and Jarmain, C. 2014. Quantification of transmission processes along the Letaba River for improved delivery of environmental water requirements (Ecological Reserve). *Water Research Commision Report Deliverable No. 1: Project K5/2338/1*.

Su, Z and Wang, L. 2013. Earth Observation of Water Resources (SEBS). Practical Session Instructions (July 2013). ITC. University of Twente. The Netherlands.

Su, Z, Schmugge, T, Kustas, WP and Massman, WJ. 2001. An evaluation of two models for estimation of the roughness height for heat transfer between the land surface and the atmosphere. *Journal of Applied Meteorology* 40(10): 1933-1951.

Su, Z. 2002. The Surface Balance Energy System (SEBS) for estimating turbulent heat fluxes. *Hydrology and Earth System Sciences*. 6(1): 85-99.

Su, Z, Pelgrum, H, and Menenti, M. (1999). Aggregation effects of surface heterogeneity in land surface processes. *Hydrology Earth System Sci*ence 3(4): 549-563.

Timmermans, J. 2014. Personal communication. International Institute of Geo-information sciences and Earth Observation (ITC). Pietermaritzburg. South Africa. 23/09/2014.

United States Geological Survey (USGS). 2015. Landsat 8 (l8) Data Users Handbook. Version 1.0. June 2015.

Van Dijk, AI and Renzullo, LJ. 2011. Water resource monitoring systems and the role of satellite observations. *Hydrology and Earth System Science* 15: 39–55.

Xu, X, Li, J and Tolson, BA. 2014. Progress in integrating remote sensing data and hydrologic modelling. *Progress in Physical Geography* 38(4): 464–498.

Yang, D, Chen, H and Lei, H. 2010. Estimation of evapotranspiration using a remote sensing model over agricultural land in the North China Plain. *International Journal of Remote Sensing* 31(14): 3783–3798.

Zhuo, G, Ba, L, Ciren, P and Bu, L. 2014. Study on daily surface evapotranspiration with SEBS in Tibet Autonomous Region. *Journal of Geographical Sciences* 24(1): 113-128.

3. ESTIMATING OPEN WATER EVAPORATION ALONG A PORTION OF THE GROOT LETABA RIVER

3.1 Introduction

There are numerous techniques which have been employed to estimate open water evaporation, in South Africa. These include techniques, inter alia; such as; (a) water balance or mass transport equations, (b) simple energy budget methods, (c) pan methods and (d) micrometeorological methods (Jarmain et al.. 2009a).

Micrometeorological approaches such as the Eddy covariance and Bowen Ratio technique, can provide good measurements of open water evaporation, using an energy balance approach (Everson. 1999). While, these techniques would be ideally suited for the estimation of open water evaporation in this study, they were not selected for application. This decision was largely based on the; (i) availability of equipment during the various monitoring periods for the study, (ii) financial and human resources available, to purchase and maintain the necessary equipment and sensors. Furthermore, the nature and remote location of the study area, would pose limitations to the routine maintenance and monitoring of sensors.

The installation of an Automatic Weather Station (AWS) in close proximity to the river for the study, facilitates the application of simple energy budget approaches (indirect methods) for the estimation of open water evaporation. Some of the commonly applied techniques are the Priestley-Taylor method (Priestley and Taylor. 1972). Penman potential evaporation equation (Penman. 1948) and Penman-Monteith reference evapotranspiration method (Allen et al.. 2006). These techniques generally provide accurate estimates of open water evaporation provided, representative meteorological data is used during the estimation procedure (Everson. 1999; Jarmain *et al*.. 2009a).

3.2 The Priestley Taylor method

The Priestley-Taylor method was selected for application in this study (Priestley and Taylor. 1972). The selection of this technique was based on the results obtained for the study undertaken by Everson (1999) along the Orange River. Everson (1999) showed that the open water evaporation estimates obtained from the Priestley Taylor method can be applied to a large river flowing through an arid region.

However, the successful application of technique largely centres on the weather station data being representative of the prevailing conditions over the open water surface (Jarmain *et al*.. 2009a).

According to Xu and Singh (2002) the technique developed by Priestley and Taylor (1972) represents a simplified version of the combination equation discussed in Penman (1948) and is applied for surfaces that are generally wet, a condition required for potential evaporation.

The Priestley-Taylor method excludes the aerodynamic component of the Penman (1948) equation and multiplies the energy component by a coefficient (α =1.26). for surrounding areas which are experiencing wet or humid conditions (Xu and Singh. 2002).

3.3 Methodology

The Priestley-Taylor equation is given as;

$$ET = \alpha\left(\frac{\Delta}{\Delta+\gamma}\right)\left(\frac{R_n-G_o}{\lambda}\right) \quad (3.1)$$

Where ET is the open water evaporation (mm day^{-1}). R_n is the net radiation (MJ m^2 day^{-1}). G_o is the soil heat flux density (MJ m^2 day^{-1}). γ is the psychometric constant (kPa $^oC^{-1}$). Δ is the slope of the vapour pressure curve (kPa $^oC^{-1}$) and λ is the latent heat of vaporization (2.45 MJ kg^{-1}).

Meteorological data required for the estimation of open water evaporation was obtained from sensors installed within the river channel to monitor meteorological conditions as well as the components of the shortened energy balance. The net radiation component of the shortened energy balance was measured using a NR Lite net radiometer installed at approximately 2 m above the water surface.

The soil heat flux density for an open water body was measured using soil heat flux plates and soil temperature sensors. The soil heat flux plates and the soil temperature sensors were attached to a metal rod and inserted into the water to collect measurements at a depth of 80 mm. 20 mm and 60 mm respectively. These measurements were then used in conjunction with ancillary data to determine the soil heat flux density.

The sensors installed within the river channel to monitor meteorological conditions were installed at two separate points along the Groot Letaba River between Letaba Ranch and Mahale weirs, during the period of study. The system was first setup within the river channel nearby a farm and measurements were acquired from the 17th Jun to 13th Aug 2015. The system was then moved to a protected area (livestock prevented from grazing) approximately 1.2 km further upstream within the river channel nearby a lodge and measurements were acquired from the 21st Aug to 22nd Oct 2015. Measurements of meteorological variables were taken at 10 minute intervals. These measurements were summed to daily values and were used for the estimation of the open water evaporation, using Equation 3.1.

3.4 Results

The results of the open water evaporation estimation using Equation 3.1 are presented in Table 3.1 and illustrated in Figure 3.1. The total open water evaporation estimated during the period of study was 208 mm. with an average of 1.63 mm of open water being evaporated daily.

Table 3.1 A statistical evaluation of the open water evaporation for a portion of the Groot Letaba River, estimated using the Priestley-Taylor technique for the period 17th Jun to 22nd Oct 2015

Open Water Evaporation (mm)	
Total	208.03
Average	1.63
Max	4.61
Min	0.03
Median	1.64
Variance	1.11
Std Dev	0.50

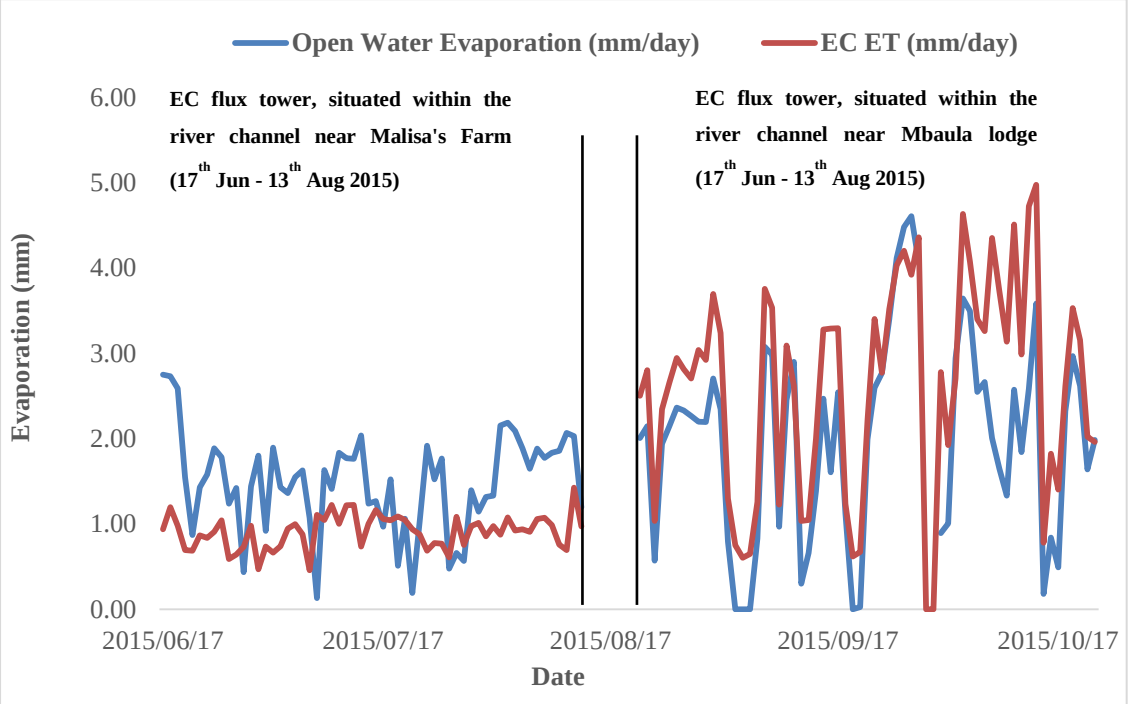

Figure 3.1 Open water evaporation for a portion of the Groot Letaba River. estimated using the Priestley-Taylor technique for the period 17th Jun to 22nd Oct 2015 (A value of 0 mm/d is indicative of periods when no data was available)

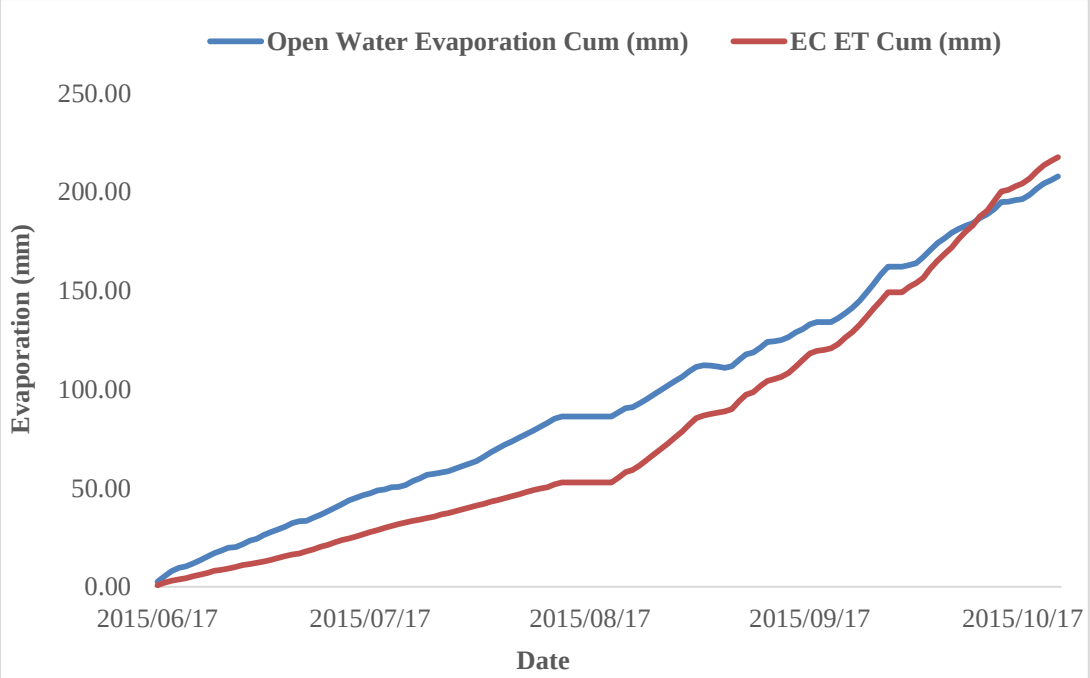

Figure 3.2 A comparison of *in-situ* total evaporation estimates acquired from an EC flux tower. and open water evaporation for the period 17th June to 22nd October 2015

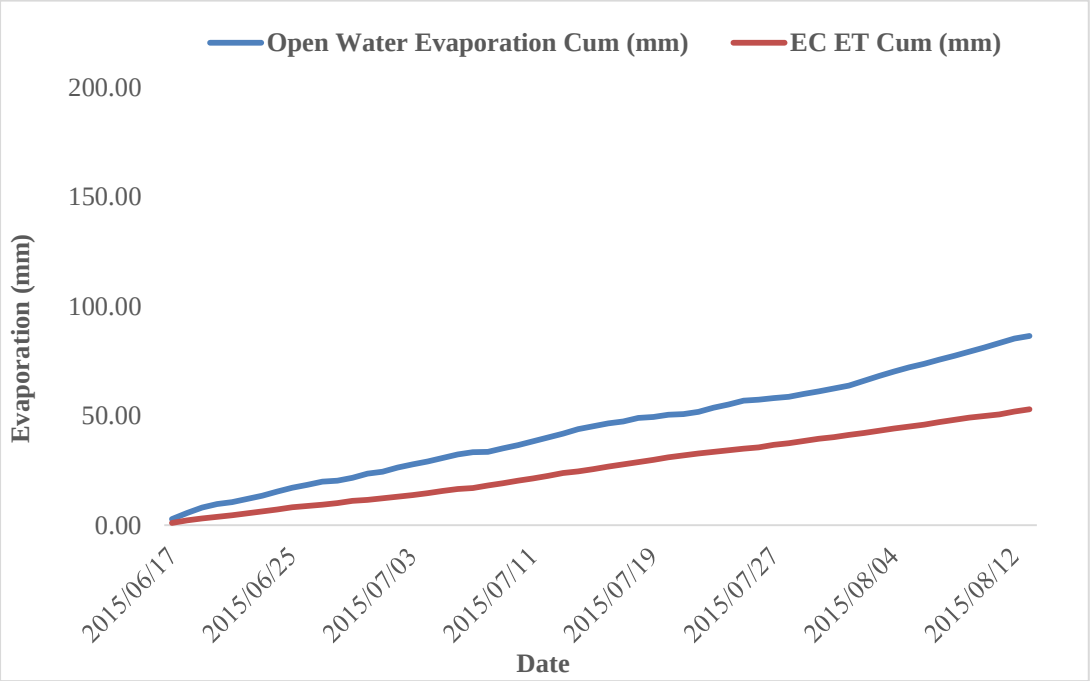

Figure 3.3 A comparison of *in-situ* total evaporation estimates acquired from an EC flux tower and open water evaporation for the period 17th June to 13th Aug 2015

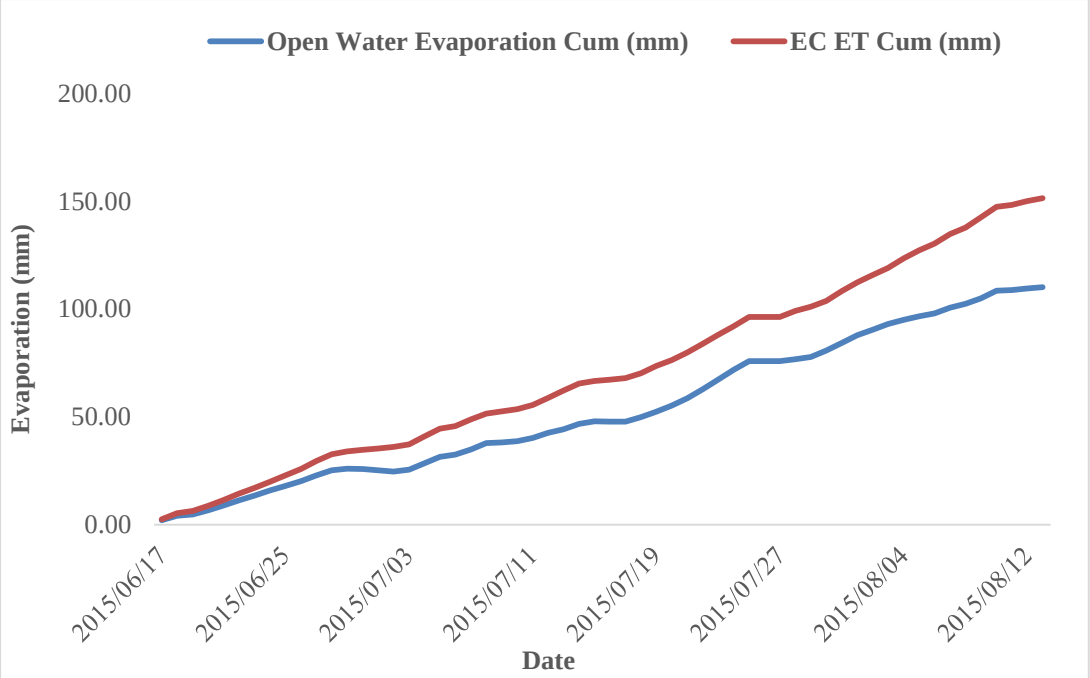

Figure 3.4 A comparison of *in-situ* total evaporation estimates acquired from an EC flux tower and open water evaporation for the period 21st Aug to 22nd Oct 2015

REFERENCES

Everson, CS. 1999. Evaporation from the Orange River: quantifying open water resources. *WRC Report No*. 683/1/99. ISBN No. 1 86845 520 3.

Jarmain, C, Everson. CS. Savage. MJ. Mengistu. MG. Clulow. AD. Walker. S and Gush. MB. 2009a. Refining tools for evaporation monitoring in support of water resources management. *WRC Report No* 1567/1/08. ISBN 978-1-77005-798-2.

Penman, HL. 1948. Natural evaporation from open water. bare soil and grass. *Proc Royal Soc* 1032: 120-145.

Priestley, CHB and Taylor RJ, 1972. On the assessment of surface heat flux and evaporation using large-scale parameters. *Monthly Weather Review* 100: 81–92.

Xu, CY and Singh, VP. 2002. Cross comparison of empirical equations for calculating potential evapotranspiration with data from Switzerland. *Water Resources Management* 16: 197–219.

4. ESTIMATING SOIL WATER EVAPORATION

Micro Lysimeter measurements were taken to determine the rate of soil water evaporation within the river channel at selected points for transect 1 and transect 2. The micro-lysimeters were made of 2 mm thick PVC pipe, were 100 mm deep and had an internal diameter of 50 mm. Each micro-lysimeter was equipped with one external cylinder made of 3 mm thick PVC pipe which was 80 mm in diameter and 145 mm deep. The external cylinders were placed at fixed positions, whilst the internal cylinders were filled with soil samples extracted from selected areas within the river channel. Extraction of soil samples from the top soil layer was typically done at the start of the day, generally around 09:00 AM. The rate of soil water evaporation can be calculated as;

$$E_s = \frac{\Delta \text{Mass} * 10^{-3}}{A} \quad (4.1)$$

Where *ΔMass* is the mass of the soil sample (g) and *A* is the surface area of the micro-lysimeter (0.0196 m^2)

The micro-lysimeter measurements were conducted for three separate campaigns. in order to account for variations in soil water evaporation at different locations within the river channel. as well as for varying climatic conditions.

4.1 Estimating soil water evaporation within the river channel at transect 1

Six sampling points were selected at approximately 5 m intervals from the river channel, in order to obtain a representative soil water evaporation estimate across the river channel. The micro-lysimeters were filled with moist soil and their initial mass was recorded. Thereafter, hourly measurements of their mass was recorded. The hourly recordings of mass are presented in Table 4.1, whilst Figure 4.1 and Table 4.2, present the rate of soil water evaporation.

Table 4.1 Change in mass of soil samples per hour, during clear sky and hot conditions on the 13th August 2015

Mass of Samples (g)						
	Inner Channel		**Mid Channel**		**Far end of Channel**	
Time	**Lys 1**	**Lys 2**	**Lys 3**	**Lys 4**	**Lys 5**	**Lys 6**
09:00 AM	142.525	141.600	149.975	138.640	147.400	146.235
10:00 AM	142.245	141.300	149.640	138.585	147.020	145.860
11:00 AM	141.900	141.075	149.300	138.550	146.770	145.600
12:00 PM	141.550	140.810	148.890	138.525	146.390	145.250
01:00 PM	141.070	140.580	148.480	138.470	145.960	144.850
02:00 PM	140.600	140.525	148.135	138.470	145.560	144.545
03:00 PM	140.300	140.285	147.845	138.370	145.120	144.190

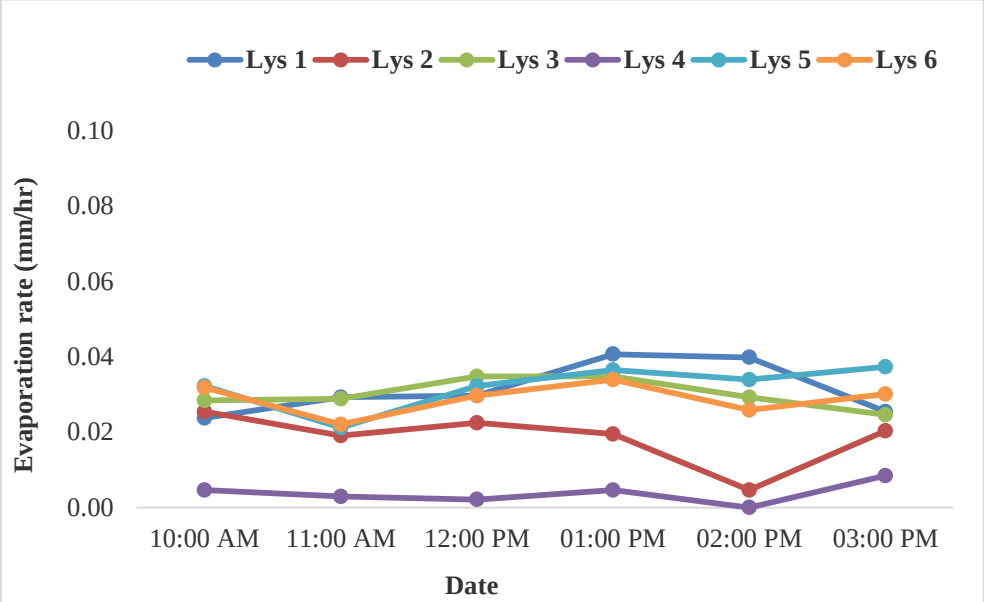

Figure 4.1 Rate of soil water evaporation for clear sky and hot conditions on the 13th August 2015

Table 4.2 Rate of soil water evaporation for clear sky and hot conditions on the 13th August 2015

Soil Water Evaporation (mm/hr)						
	Inner Channel		**Mid Channel**		**Far end of Channel**	
Time	**Lys 1**	**Lys 2**	**Lys 3**	**Lys 4**	**Lys 5**	**Lys 6**
10:00 AM	0.02	0.03	0.03	0.00	0.03	0.03
11:00 AM	0.03	0.02	0.03	0.00	0.02	0.02
12:00 PM	0.03	0.02	0.03	0.00	0.03	0.03
01:00 PM	0.04	0.02	0.03	0.00	0.04	0.03
02:00 PM	0.04	0.00	0.03	0.00	0.03	0.03
03:00 PM	0.03	0.02	0.02	0.01	0.04	0.03
Total	**0.19**	**0.11**	**0.18**	**0.02**	**0.19**	**0.17**

The soil water evaporation was estimated by averaging the total soil water evaporation measured for the six sampling points. Approximately 0.15 mm of water was evaporated from the soil surface during clear sky and hot conditions within the river channel at transect 1 on the 13th of August 2015.

4.2 Estimating soil water evaporation within the river channel at transect 2

Soil water evaporation measurements were taken from 30th September to 02nd October 2015. Three sampling points were selected in close proximity to the river channel, approximately within 7 m. The micro-lysimeters were filled with moist soil and their initial mass was recorded. Thereafter, hourly measurements of their mass was recorded. The hourly recordings of mass are presented in Table 4.3, whilst Figures 4.2. 4.3. 4.4 and Table 4.4 the rate of soil water evaporation.

Table 4.3 Change in mass of soil samples per hour on the 30th September. 01st October and 02nd October 2015

Mass of Samples (g) on the 30th September 2015 for hot and clear sky conditions			
	Near River Channel		
Time	**Lys 1**	**Lys 2**	**Lys 3**
09:00 AM	308.160	327.970	374.710
10:00 AM	306.800	327.700	373.660
11:00 AM	304.990	326.100	371.980
12:00 PM	303.070	324.950	370.400
01:00 PM	301.110	323.960	368.760
02:00 PM	299.250	323.050	367.120
03:00 PM	297.670	322.560	365.840
04:00 PM	296.450	322.060	364.720
Mass of Samples (g) on the 01st October 2015 for hot and clear sky conditions			
	Near River Channel		
Time	**Lys 1**	**Lys 2**	**Lys 3**
08:00 AM	340.28	347.52	398.64
09:00 AM	340.010	347.300	398.480
10:00 AM	338.980	346.430	397.540
11:00 AM	337.140	344.980	396.120
12:00 PM	335.360	343.480	394.720
01:00 PM	333.190	341.710	393.060
02:00 PM	331.540	340.320	391.680
03:00 PM	329.940	339.040	390.420
04:00 PM	328.680	338.030	389.440
Mass of Samples (g) on the 02nd October 2015 for cloudy and windy conditions			
	Near River Channel		
Time	**Lys 1**	**Lys 2**	**Lys 3**
09:00 AM	387.420	395.310	420.010
10:00 AM	386.750	394.720	419.050

11:00 AM	385.680	393.820	418.020
12:00 PM	384.570	392.870	417.090
01:00 PM	383.220	391.810	415.800
02:00 PM	381.830	390.800	414.600
03:00 PM	380.430	390.000	413.350
04:00 PM	379.140	389.220	412.110

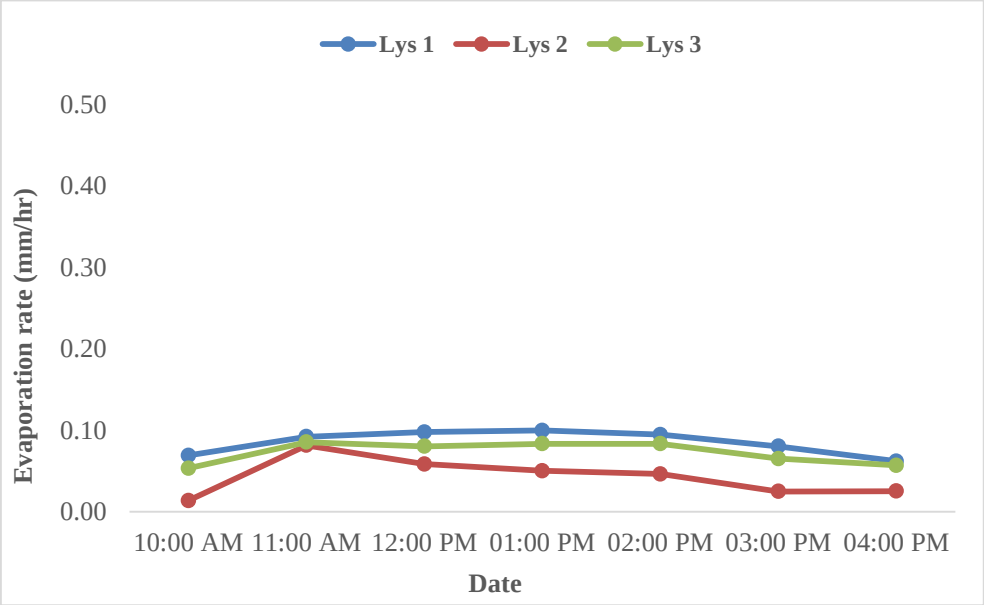

Figure 4.2 Rate of soil water evaporation for clear sky and hot conditions on the 30th September 2015

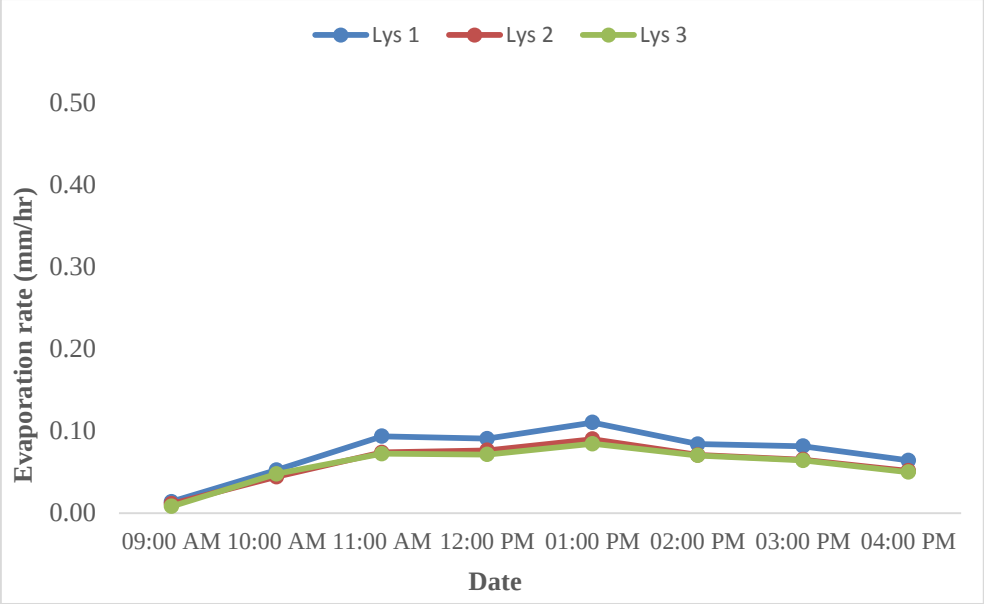

Figure 4.3 Rate of soil water evaporation for clear sky and hot conditions on the 01st October 2015

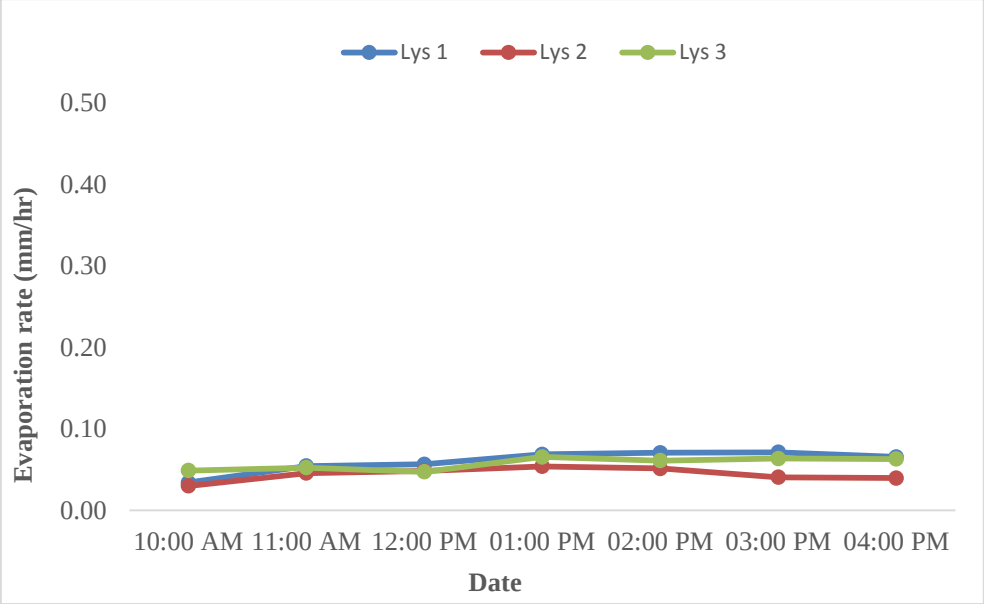

Figure 4.4 Rate of soil water evaporation for cloudy and windy conditions on the 02nd October 2015

Table 4.4 Rate of soil water evaporation on the 30th September. 01st October and 02nd October 2015

Soil Water Evaporation (mm/hr) on the 30th September 2015 for hot and clear sky conditions			
	Near River Channel		
Time	**Lys 1**	**Lys 2**	**Lys 3**
10:00 AM	0.07	0.01	0.05
11:00 AM	0.09	0.08	0.09
12:00 PM	0.10	0.06	0.08
01:00 PM	0.10	0.05	0.08
02:00 PM	0.09	0.05	0.08
03:00 PM	0.08	0.02	0.07
04:00 PM	0.06	0.03	0.06
Total	**0.60**	**0.30**	**0.51**
Soil Water Evaporation (mm/hr) on the 01st October 2015 for hot and clear sky conditions			
	Near River Channel		
Time	**Lys 1**	**Lys 2**	**Lys 3**
09:00 AM	0.01	0.01	0.01
10:00 AM	0.05	0.04	0.05
11:00 AM	0.09	0.07	0.07
12:00 PM	0.09	0.08	0.07
01:00 PM	0.11	0.09	0.08
02:00 PM	0.08	0.07	0.07
03:00 PM	0.08	0.07	0.06
04:00 PM	0.06	0.05	0.05
Total	**0.59**	**0.48**	**0.47**
Soil Water Evaporation (mm/hr) on the 02nd October 2015 for cloudy and windy conditions			
	Near River Channel		
Time	**Lys 1**	**Lys 2**	**Lys 3**
10:00 AM	0.03	0.03	0.05
11:00 AM	0.05	0.05	0.05
12:00 PM	0.06	0.05	0.05
01:00 PM	0.07	0.05	0.07
02:00 PM	0.07	0.05	0.06
03:00 PM	0.07	0.04	0.06
04:00 PM	0.07	0.04	0.06
Total	**0.42**	**0.31**	**0.40**

The soil water evaporation was estimated by averaging the total soil water evaporation measured for the three sampling points. Approximately 0.47 mm. 0.51 mm and 0.38 mm of water was evaporated from the soil surface within the river channel at transect 2 on the 30th September. 01st October and 02nd October 2015, respectively.

Soil water evaporation measurements were once again taken within the river channel at transect 2 on the 07th October 2015. However, unlike the measurements conducted from the 30th September to 02nd October 2015, the sampling points were situated further away from the river channel. This was done in order to assess the evaporation rates from soils further away from the river. The sampling points where situated at approximately 7 m intervals away from the river channel.

The micro-lysimeters were filled soil samples extracted in close proximity to the sampling points and their initial mass was recorded. Thereafter, hourly measurements of their mass was recorded. The hourly recordings of mass are presented in Table 4.5, whilst Figure 4.5 and Table 4.6 present the rate of soil water evaporation.

Table 4.5 Change in mass of soil samples per hour, during clear sky and hot conditions on the 07th October 2015

Mass of Samples (g)			
	Mid Channel 1 (7 m)	**Mid Channel 2 (13 m)**	**Far end of Channel (19 m)**
Time	**Lys 1**	**Lys 2**	**Lys 3**
09:00 AM	333.010	302.710	334.550
10:00 AM	332.200	302.120	334.400
11:00 AM	332.070	300.780	334.280
12:00 PM	331.060	300.680	334.270
01:00 PM	331.100	300.220	334.230
02:00 PM	330.940	300.140	334.120
03:00 PM	330.200	300.010	334.030
04:00 PM	329.720	299.940	333.970

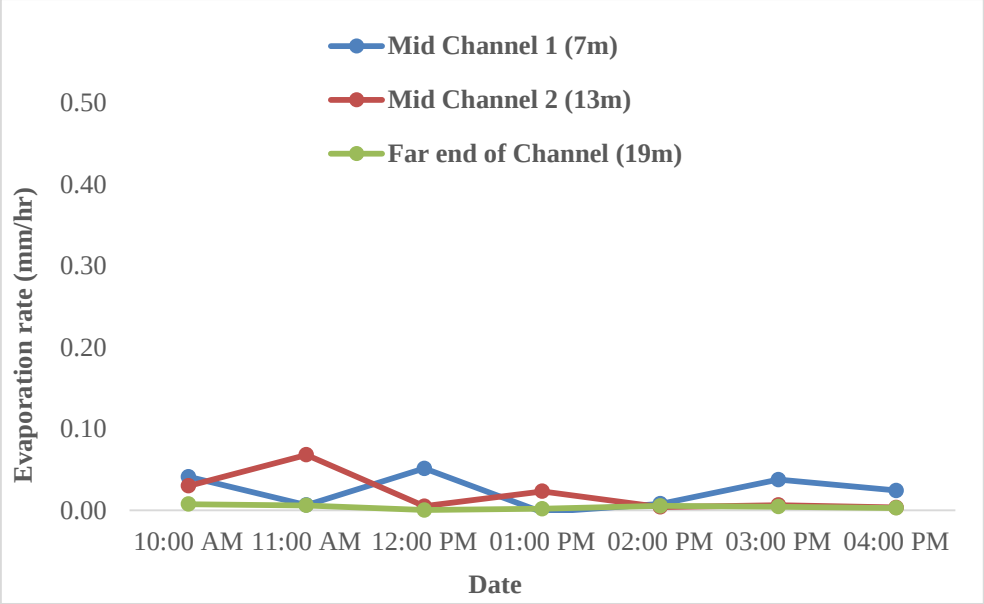

Figure 4.5 Rate of soil water evaporation for clear sky and hot conditions on the 07th October 2015

Table 4.6 Soil Water Evaporation

Soil Water Evaporation (mm/hr)			
	Mid Channel 1 (7m)	**Mid Channel 2 (13m)**	**Far end of Channel (19m)**
Time	**Lys 1**	**Lys 2**	**Lys 3**
10:00 AM	0.04	0.03	0.01
11:00 AM	0.01	0.07	0.01
12:00 PM	0.05	0.01	0.00
01:00 PM	0.00	0.02	0.00
02:00 PM	0.01	0.00	0.01
03:00 PM	0.04	0.01	0.00
04:00 PM	0.02	0.00	0.00
Total	**0.17**	**0.14**	**0.03**

The soil water evaporation was estimated by averaging the total soil water evaporation measured for the three sampling points. Approximately 0.11 mm of water was evaporated from the soil surface within the river channel at transect 2 on the 07th October 2015.

The soil water evaporation obtained for 07th October 2015, is evidently lower than the soil water evaporation obtained during the period from 30th September to 02nd October 2015. This is largely attributed to the soil being drier in the middle and far end of the river channel. Furthermore the intense heat wave, experienced during this time could have

contributed to a significant decrease in the moisture levels of the soil from the time of the last measurement.

The results of the investigations have shown that there is a contribution of soil water evaporation, to the total evaporation. However, this contribution is fairly low. There does exist marginal variations in the soil water evaporation at different locations and for different climatic conditions.

It should be noted that EC total evaporation estimates are weighted according to the coverage of land uses across the area in which the system is situated, therefore an area associated with a large percentage coverage of bare soil will potentially possess lower total evaporation values. The results presented within here can be used to assist with the interpretation of the EC total evaporation, however only a few measurements of soil water evaporation have been conducted and these measurements are not necessarily representative of the conditions for the duration of the study period.

5. WORKPLAN

- Installation of EC flux tower and Meteorological sensors within the river channel, as well as ancillary investigation, such as measurement of soil water evaporation.
- Satellite earth observation data acquisition and processing.
- Landcover classification and determination of water usage for individual riparian species.
- Geophysics.
- Isotope.

Appendix I Reference ET in surrounding landscape

Figure I.1 Location of DAVIS Vantage Pro automatic weather stations (yellow pins) in relation to the Eddy Covariance station sites (blue markers).

Appendix II Comparison of In-situ and Satellite ET with Mass Balance Methods

In deliverable 3 (July 2015), mass balance approaches were described to estimate ET losses from the river reach between Mahale Weir and Letaba Ranch (B8H008) weir, using the method of Mayboom (1965) to infer daily ET from the baseflow response of the river using raw data from B8H008. Unfortunately due to instrumentation problems at that gauge this analysis could not be extended (at time of writing). However the initial Mayboom methods calculations are plotted against the satellite derived ET data presented in this report by way of comparison. It is clear from the Figure II.1 that the Mayboom ET corresponds more closely with the Landsat ET between 26 June 2015 and 8 July 2015m whilst being greater than the downscaled ET method. Note that after 10 July 2015 the Mayboom ET increases significantly due to flow increases in the river – reported in previous deliverable as reduced upstream irrigation abstraction. Thereafter the Mayboom ET still follows the Landsat ET.

It is hoped that this analysis can be continued once data verification for B8H008 has been completed by the Department of Water & Sanitation.

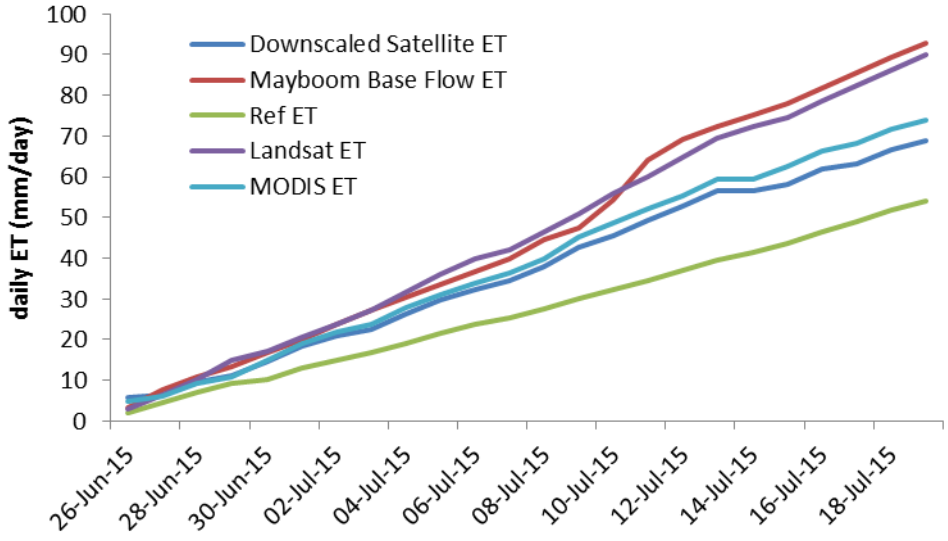

Figure II.1 Comparison of the satellite (SEBS) derived cumulative daily ET with the Mayboom baseflow ET method.

Appendix III UAV Aerial Survey

Figure III.1 An Unmanned Aerial Vehicle survey conducted of the Letaba river study site around the Eddy Co-Variance installation area during November 2015.